
Weakly interacting electrons and the renormalization group

Benedikt Binz^{*1,2}, **Dionys Baeriswy**¹, and **Benoît Douçot**³

¹ Département de Physique, Université de Fribourg, Pérolles, CH-1700 Fribourg, Switzerland

² Theoretische Physik, ETH Zürich, CH-8093 Zürich, Switzerland

³ Laboratoire de Physique Théorique et Hautes Energies, CNRS UMR 7589, Universités Paris VII, 4 Place Jussieu, 75252 Paris Cedex 05, France

Key words Correlated electrons, Hubbard model, parquet summation, renormalization group, superconductivity

PACS 05.10.Cc, 05.30.Fk, 71.10.Fd, 74.20.Mn

We present a general method to study weak-coupling instabilities of a large class of interacting electron models in a controlled and unbiased way. Quite generally, the electron gas is unstable towards a superconducting state even in the absence of phonons, since high-energy spin fluctuations create an effective attraction between the quasi-particles. As an example, we show the occurrence of d -wave pairing in the repulsive Hubbard model in two dimensions. In one dimension or if the Fermi surface is nested, there are several competing instabilities. The required renormalization group formalism for this case is presented to lowest (one-loop) order on a most elementary level, connecting the idea of the “parquet summation” to the more modern concept of Wilson’s effective action. The validity and restrictions of the one-loop approximation are discussed in detail. As a result, three different renormalization group approaches known in the literature are shown to be equivalent within the regime of applicability. We also briefly discuss the open problem of a two-dimensional Fermi system at Van Hove filling without nesting.

Contents

1	Introduction	2
2	Infrared divergences in naïve perturbation theory	3
3	Ladder approximation and BCS theory	6
4	Superconductivity from repulsive interactions	8
5	Nesting	11
6	Bethe-Salpeter equations	11
7	RG flow of the vertex	15
8	Discussion of the low-energy behavior	17
9	Relation to the Wilsonian approach	18
10	Other one-loop RG equations	20
11	Conclusion	22
A	Definition and properties of the vertex function	24
B	Parquet diagrams: An example	25
C	Linear response	26
C.1	Generalized susceptibilities for superconductivity	27
C.2	Density waves and flux phases	28
C.3	Flow equations for the susceptibilities	30

* Corresponding author: E-mail: benedikt.binz@unifr.ch, Phone: +41 26 300 91 41, Fax: +41 26 300 97 58

D Functional integral formulation	31
References	32

1 Introduction

The theoretical understanding of systems with strongly correlated electrons is one of the most important objectives of current research in physics and the key for elucidating a number of phenomena which have been observed in newly designed materials. The most spectacular example is obviously high-temperature superconductivity discovered 1986 in the cuprates, but intriguing questions have also been raised by other transition metal oxides, by organic compounds etc.

Although the (bare) Coulomb interaction between electrons is generally strong in materials, it is important to control at least the limit of weak interactions, which is already a difficult task. Furthermore, arbitrarily weak interactions lead to strong correlations at low temperature. It is thus worthwhile to study the weak-coupling problem thoroughly.

As will be shown in detail, naïve perturbation theory breaks down at low temperature and has to be improved by the so-called renormalization group (RG). RG concepts have been used in very different fields of modern physics and can have quite different meanings for different people. The notion was first introduced by Stückelberg and Petermann [SP53] and independently by Gell-Mann and Low [GM54] in the context of quantum field theories (such as quantum electrodynamics) in order to cope with infinities that appear in naïve perturbation theory.

In the early 1970s, Kadanoff and Wilson have associated the RG to the procedure of mode elimination in classical statistical mechanics (or systems of bosons) [Wil71, WK74]. In Wilson's formulation, the RG transformation consists in integrating out some degrees of freedom of the system and including them in the renormalization of some parameters (for example coupling constants). This alternative formulation of the RG idea proved tremendously successful for the analysis of critical behavior in the vicinity of second order phase transitions [Wil75].

In general, a RG transformation is some change of the length or energy scale and the RG equations describe the response of the system as the length or energy scale is changed. In the interacting electron problem considered here, the energy scale is given by the temperature or alternatively by a cutoff Λ in the band energy of the electrons. The RG equations describe the change of a two-particle Green's function as a function of the energy scale Λ . In many cases, the RG flow to low energies produces a singularity at a finite energy scale Λ_c . This is interpreted as a transition into a strongly correlated state. The energy scale Λ_c is then comparable to the mean-field transition temperature towards an ordered state.

It turns out that the one-loop (i.e. the leading order) approximation of the RG is equivalent to the so-called parquet approximation. This method was developed by the soviet school [PSTM56] in order to treat different diverging fluctuations on an equal footing. It was successfully applied to one-dimensional conductors [BGD66, DK72, GD74], to the Kondo problem [Abr65] and to the X -ray absorption edge singularity problem in metals [RGN69, NGR69]. A detailed description of the method can be found in [RGN69]. In our derivation of the one-loop RG equations, we will follow mainly the parquet philosophy.

The application of renormalization group (RG) ideas to fermionic problems in more than one dimension started in the mathematical physicists community [FT90, BG91] and has led to a considerable progress during the last decade¹. For example, a series of rigorous studies has shown that the Landau Fermi liquid theory is stable for the D=2 jellium model at not too low temperatures such that $|U \log T| < \text{const}$, where U is the strength of the local interaction [Sal98, DR00]. For lower temperatures, the properties of the interacting system are no longer analytically connected to those of the non-interacting system. The usual

¹ Pedagogical introductions can be found in [Pol92, Sha94, CFS96]. A precise relationship between Fermi liquid theory and the renormalization group has been established in [CS95, CS98, Dup98, Dup00].

interpretation is a phase transition into a superconducting state, although there exists so far no rigorous statement about the regime $T < T_c$.

A number of different numerical schemes to compute the one-loop RG flow of D=2 Fermion models have been developed during the last years. They have revealed many interesting and appealing results such as the appearance of d -wave superconductivity in the repulsive Hubbard model close to half filling [Zan96, ZS00], a spontaneous breaking of the lattice symmetry (Pomeranchuk instability) [HM01] and a phase with suppressed uniform spin and charge susceptibilities (“insulating spin liquid”) [HSFR01]. The method was further developed to a finite temperature RG scheme in [HS01a]. An interesting extension of the RG formalism to obtain dynamical and non-equilibrium properties of certain impurity models has been presented in Ref. [RPKW03].

In this article, we have chosen a comparatively pedestrian approach to the weakly interacting electron problem and its RG treatment with the aim of being intuitive and didactical. The paper is organized as follows. In Section 2, we show how naïve perturbation theory breaks down as a consequence of infrared divergences. In the case of a generic Fermi surface in more than one dimension, these divergences can be accounted for in a controlled way using the ladder approximation. This method is presented in section 3, where we also discuss its relation to Kohn-Luttinger superconductivity and BCS-theory. This part is followed by a specific application in section 4, showing the occurrence of superconductivity in the repulsive Hubbard model in two dimensions.

The remaining part of this article addresses the more general situation, where there is more than one competing weak coupling instability. This is generally the case in one dimension and in more than one dimension for special (nested) Fermi surfaces, which are defined in section 5. If the Fermi surface is nested, the ladder approximation is no longer justified and requires a non trivial extension. The necessary formalism is developed in Sections 6 and 7. We first derive several exact Bethe-Salpeter equations which are then used to establish the one-loop RG equations. The region of applicability of the one-loop RG is discussed in section 8. In section 9, we relate our approach to the Wilsonian RG concept and we finally compare several recent RG approaches known in the literature in section 10. In the Conclusion, we comment upon two-dimensional electron systems at the Van Hove filling.

Some more technical aspects are treated in four appendices. Appendix A contains basic definitions and properties of the two-particle Green’s function and the vertex function. In Appendix B, we calculate a specific example of a third order parquet diagram, in order to demonstrate the general properties to which the main text refers. In Appendix C, the RG formalism is extended to calculate linear response functions. Finally, some basic definitions and identities of the functional integral formulation are given in Appendix D.

2 Infrared divergences in naïve perturbation theory

We consider a general single-band model of interacting electrons on a d -dimensional periodic lattice. The Hamiltonian is of the form $H = H_0 + H_I$, where

$$H_0 = \sum_{\mathbf{k}, \sigma} \epsilon_{\mathbf{k}} c_{\mathbf{k}\sigma}^\dagger c_{\mathbf{k}\sigma} \quad (1)$$

is the non-interacting part and

$$H_I = \frac{1}{2V} \sum_{\mathbf{k}_1, \mathbf{k}_2, \mathbf{k}_3} g(\mathbf{k}_1, \mathbf{k}_2, \mathbf{k}_3) \sum_{\sigma, \sigma'} c_{\mathbf{k}_1 \sigma}^\dagger c_{\mathbf{k}_2 \sigma'}^\dagger c_{\mathbf{k}_3 \sigma'} c_{\mathbf{k}_1 + \mathbf{k}_2 - \mathbf{k}_3 \sigma}, \quad (2)$$

is the most general two-body interaction respecting the global spin rotation symmetry, translational invariance and particle number conservation. V is the number of lattice sites (i.e. the system volume), $c_{\mathbf{k}\sigma}^\dagger$ and $c_{\mathbf{k}\sigma}$ are the usual creation and annihilation operators of electrons with lattice momentum \mathbf{k} and spin index

$\sigma = \uparrow, \downarrow$. The single-particle dispersion ϵ and the coupling function g are smooth functions of the momenta, if the hopping matrix and the interactions are short-ranged in real space.

Our aim is to calculate the imaginary time Green's functions. Special attention is given to the vertex function $\Gamma(k_1, k_2, k_3)$, which is defined as the one-particle irreducible part of the two-particle Green's function. The $d+1$ -dimensional frequency-momentum vectors $k_i = (k_{0i}, \mathbf{k}_i)$, involve the Matsubara frequencies k_{0i} which run over the odd multiples of π/β , where β is the inverse temperature. $\Gamma(k_1, k_2, k_3)$ represents a scattering amplitude of two particles with incoming frequency-momentum and spin labels (k_1, \uparrow) and (k_2, \downarrow) into outgoing labels (k_3, \downarrow) and $(k_1 + k_2 - k_3, \uparrow)$. A precise definition of the vertex function as well as some basic symmetry properties are given in Appendix A.

The vertex is always a regular function at high enough temperatures. At low temperatures however, the vertex can have poles. These poles are usually interpreted as the manifestation of an instability of the metallic state such as superconductivity or different kinds of density waves, since a divergence of the vertex implies a divergence of some generalized susceptibility.

Since we are concerned with weak interactions, the first approach is standard perturbation theory in H_I . A calculation of the vertex function to second order in perturbation theory gives

$$\Gamma(k_1, k_2, k_3) = -g(\mathbf{k}_1, \mathbf{k}_2, \mathbf{k}_3) + \text{PP} + \text{PH1} + \text{PH2} \quad (3)$$

$$\begin{aligned} \text{PP} &= \frac{1}{\beta V} \sum_p g(\mathbf{k}_1, \mathbf{k}_2, \mathbf{k} - \mathbf{p}) C(p) C(k - p) g(\mathbf{p}, \mathbf{k} - \mathbf{p}, \mathbf{k}_3), \\ \text{PH1} &= \frac{1}{\beta V} \sum_p g(\mathbf{k}_1, \mathbf{p} + \mathbf{q}_1, \mathbf{k}_3) C(p) C(p + q_1) g(\mathbf{p}, \mathbf{k}_2, \mathbf{p} + \mathbf{q}_1), \\ \text{PH2} &= \frac{1}{\beta V} \sum_p C(p) C(p + q_2) [-2g(\mathbf{k}_1, \mathbf{p}, \mathbf{p} + \mathbf{q}_2) g(\mathbf{p} + \mathbf{q}_2, \mathbf{k}_2, \mathbf{k}_3) \\ &\quad + g(\mathbf{p}, \mathbf{k}_1, \mathbf{p} + \mathbf{q}_2) g(\mathbf{p} + \mathbf{q}_2, \mathbf{k}_2, \mathbf{k}_3) + g(\mathbf{k}_1, \mathbf{p}, \mathbf{p} + \mathbf{q}_2) g(\mathbf{p} + \mathbf{q}_2, \mathbf{k}_2, \mathbf{p})], \end{aligned}$$

where $k = k_1 + k_2$, $q_1 = k_3 - k_1$, $q_2 = k_3 - k_2$ and the single-particle Green's function of the non-interacting system is given by

$$C(k) = \frac{1}{ik_0 - \xi_{\mathbf{k}}}, \quad (4)$$

where $\xi_{\mathbf{k}} = \epsilon_{\mathbf{k}} - \mu$. The representation of the second order contributions in terms of Feynman diagrams is shown in Fig. 1. The internal electron lines stand for free electron propagators C and the wavy interaction lines stand for coupling functions g , that depend on the incoming and outgoing momenta. The convention is that the spin index is conserved along the fermion lines. The minus sign in the first of the three PH2 diagrams comes from the fermion loop and the factor 2 in the same diagram from the sum over the spin index in the fermion loop. PP is referred to as the particle-particle (p-p) diagram and PH1 and PH2 as particle-hole (p-h) diagrams.

Suppose for a moment that g is constant ($= U$ in the Hubbard model). The p-p diagram is then given by g^2 multiplied by the p-p bubble

$$B^{pp}(k) = \frac{1}{\beta V} \sum_p C(p) C(k - p) \quad (5)$$

$$= \frac{1}{V} \sum_{\mathbf{p}} \frac{n(\xi_{\mathbf{p}}) + n(\xi_{\mathbf{k}-\mathbf{p}}) - 1}{ik_0 - \xi_{\mathbf{p}} - \xi_{\mathbf{k}-\mathbf{p}}}, \quad (6)$$

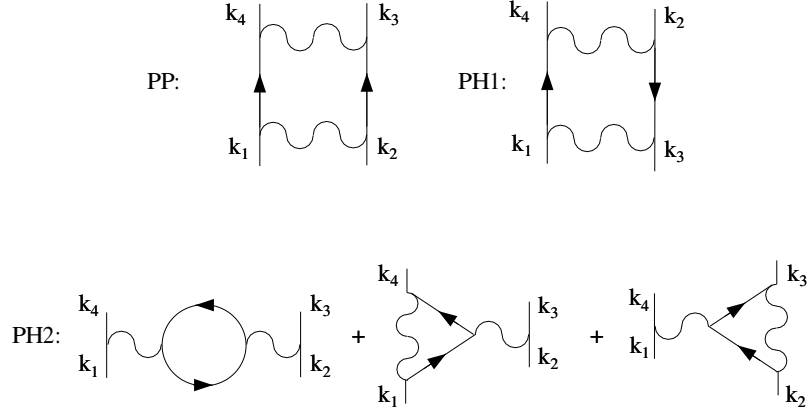


Fig. 1 Second order diagrams for the one-particle irreducible vertex $\Gamma(k_1, k_2, k_3)$. k_4 is determined by energy-momentum conservation.

where $n(\xi) = (1 + \exp \beta \xi)^{-1}$ is the Fermi distribution function. This quantity is diverging at $k = 0$ as the temperature goes to zero. At a finite temperature $T = \beta^{-1}$ one finds

$$B^{pp}(0) = \int_{-W}^W d\xi \nu(\xi) \frac{\tanh \frac{\beta \xi}{2}}{2\xi} = \nu(0) \log \frac{W}{T} + \text{"finite"}, \quad (7)$$

where W is the bandwidth, $\nu(\omega) = 1/V \sum_{\mathbf{k}} \delta(\xi_{\mathbf{k}} - \omega)$ is the density of states, and “finite” is any contribution with a finite limit $T \rightarrow 0$. The only two assumptions are reflection symmetry $\xi_{\mathbf{k}} = \xi_{-\mathbf{k}}$ and that the density of states $\nu(\xi)$ is an analytic function of ξ at the Fermi level. Under the same assumption it can be shown that the largest term of order n in the coupling diverges as $\log^{n-1}(W/T)$.

It is clear that naïve perturbation theory breaks down at large enough values of the coupling or low enough temperature, such that $|g \log(W/T)| \sim 1$. Alternatively, one can organize the perturbation series in the form

$$\Gamma = a_1 g + a_2 g^2 + \dots, \quad (8)$$

where a_1, a_2, \dots are analytic functions of the product $g \log(W/T)$. In the following we concentrate on the leading order contributions, i.e. we calculate only the first term in this expansion. This means that diagrams of a given order in g are calculated to leading logarithmic precision and all the subleading contributions such as the term “finite” in (7) are neglected. In other words, g is considered to be small, but $g \log(W/T)$ is not.

One can regularize the zero temperature perturbation theory by introducing artificially an infrared cutoff Λ . There are several ways to do this. One method of avoiding the singularity is to remove from the theory the single-particle quantum states which are too close to the Fermi surface. This amounts to replace the bare propagator by

$$C_{\Lambda}(k) = \Theta(|\xi_{\mathbf{k}}| - \Lambda) C(k), \quad (9)$$

where Θ is the Heavyside step function. In this case, the vertex function becomes cutoff-dependent and we use the notation $\Gamma_{\Lambda}(k_1, k_2, k_3)$. In the presence of the cutoff, the logarithms in Eqs. (7) and (8) are replaced by $\log \frac{W}{\max\{T, \Lambda\}}$. Alternatively, one could also use the quantity $\sqrt{k_0^2 + \xi_{\mathbf{k}}^2}$ instead of $|\xi_{\mathbf{k}}|$ to introduce the cutoff or replace Θ by a smooth function without changing the result to leading logarithmic order. We are

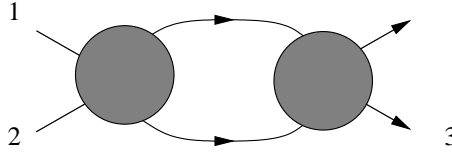


Fig. 2 The structure of diagrams, which are reducible in the p-p channel. The grey circles represent any sub-diagram.

thus free to calculate at zero temperature, introduce the cutoff in the most convenient way for calculations and in the end of the calculation replace Λ by T . Useless to say that the correspondence $\Lambda \leftrightarrow T$ is only correct to leading logarithmic order. In a more elaborate calculation including subleading contributions, the result depends on how the cutoff is introduced.

3 Ladder approximation and BCS theory

We now calculate the vertex to leading order in the expansion (8). In a generic situation in more than one dimension without any fine tuned parameter, the only diverging terms occur in the p-p diagram. The other second order terms have a finite limit $T, \Lambda \rightarrow 0$ except in one dimension or for special situations, which will be discussed later. Having identified the p-p diagram as the main source of the infrared singularity, we define the class of p-p irreducible diagrams. A diagram contributing to the two-particle scattering vertex is called reducible in the p-p channel if it is of the form shown in Fig. 2, i.e. if it can be divided into two disconnected pieces by cutting two particle lines. In the opposite case it is called irreducible in the p-p channel or simply p-p irreducible.

In the following, we use the notation $I^{pp}(k_1, k_2, k_3)$ for the sum over all p-p irreducible diagrams. To second order in perturbation theory, this quantity is given by Eq. (3) with the singular PP contribution omitted. It can thus be calculated by naïve perturbation theory without the problem of infrared divergences.

The exact full vertex is given in terms of the p-p irreducible part and the single-electron propagator by a summation over the so-called ladder diagrams (Fig. 3). The analytical expression of this series is

$$\begin{aligned} \Gamma_{\Lambda,q}^{BCS}(k, k') &= I_{\Lambda,q}^{BCS}(k, k') + \frac{1}{\beta V} \sum_p I_{\Lambda,q}^{BCS}(k, p) D_{\Lambda,q}^{pp}(p) I_{\Lambda,q}^{BCS}(p, k') \\ &\quad + \frac{1}{(\beta V)^2} \sum_{p_1, p_2} I_{\Lambda,q}^{BCS}(k, p_1) D_{\Lambda,k}^{pp}(p_1) I_{\Lambda,q}^{BCS}(p_1, p_2) D_{\Lambda,k}^{pp}(p_2) I_{\Lambda,q}^{BCS}(p_2, k') + \dots, \end{aligned} \quad (10)$$

where, q is the total frequency-momentum of the incoming and outgoing pair of particles, $D_{\Lambda,q}^{pp}(p) = G_{\Lambda}(p)G_{\Lambda}(q-p)$ is the propagator of the pair and we have defined

$$\begin{aligned} \Gamma_{\Lambda,q}^{BCS}(k, k') &= \Gamma_{\Lambda}(k, q-k, q-k'), \\ I_{\Lambda,q}^{BCS}(k, k') &= I_{\Lambda}^{pp}(k, q-k, q-k'). \end{aligned} \quad (11)$$

In principle, the internal electron propagators in Fig. 3 are exact single-particle Green's functions $G_{\Lambda}(p) = \Theta(|\xi_p| - \Lambda)/(ip_0 - \xi_p - \Sigma_{\Lambda}(p))$, where $\Sigma_{\Lambda}(p)$ is the self-energy in the presence of the cutoff. Self-energy corrections have three main effects. First they change the shape and location of the Fermi surface, second they modify the properties of the single particle dispersion (the Fermi velocity) and third they lead to a reduction of the quasi-particle weight. The deformation of the Fermi surface requires in general the introduction of counter-terms². We will ignore this effect and assume that in the weak coupling

² See Section 5.7 of Nozières' book [Noz64] for a comprehensive explanation. Rigorous mathematical statements about the moving Fermi surface have been presented in [FST96, FST98, FST99]. For recent investigations of interaction-induced Fermi surface deformations, see [DD03, LK03, NM03, Fer03].

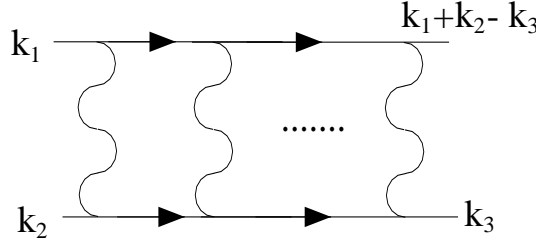


Fig. 3 The structure of p-p ladder diagrams. The wavy lines stand for $-I_{\Lambda}^{pp}$ and the electron lines represent full propagators G_{Λ} , in the presence of the infrared cutoff Λ .

limit, the interacting Fermi surface is not so different from the non interacting one such that the difference is not crucial. Perturbative corrections to the Fermi velocity $\nabla_{\mathbf{p}}\Sigma(p)$ and the quasi-particle weight $z = (1 + i\partial_{p_0}\Sigma(p))^{-1}$ are finite as $T \rightarrow 0$ and therefore do not contribute to leading logarithmic order. We will therefore neglect self-energy corrections in the remaining part of this section.

As argued above, the p-p irreducible vertex function $I_{\Lambda,q}^{BCS}$ can be calculated within naïve perturbation theory. Let us thus focus on how to sum the infinite series Eq. (10), for given $I_{\Lambda,q}^{BCS}$.

For simplicity, we set the frequency q_0 equal to zero and neglect the frequency-dependence of $I^{BCS}(k, k')$. This point will be justified later. We focus on small values of \mathbf{q} and Λ , because this is where the infrared divergence appears. The p-p irreducible vertex has no infrared singularity and can thus safely be replaced by

$$I^{BCS}(\mathbf{k}, \mathbf{k}') = \lim_{\Lambda, \mathbf{q} \rightarrow 0} I_{\Lambda, \mathbf{q}}^{BCS}(\mathbf{k}, \mathbf{k}'). \quad (12)$$

In this way, I^{BCS} becomes a real-valued and symmetric function of the momenta \mathbf{k} and \mathbf{k}' . One can then define a Hermitian operator³, which acts on a function $f(\mathbf{k})$ as

$$f(\mathbf{k}) \longrightarrow \frac{1}{VB_{\Lambda}^{pp}(\mathbf{q})} \sum_{\mathbf{k}'} I^{BCS}(\mathbf{k}, \mathbf{k}') \tilde{D}_{\Lambda, \mathbf{q}}^{pp}(\mathbf{k}') f(\mathbf{k}'), \quad (13)$$

where $\tilde{D}_{\Lambda, \mathbf{q}}^{pp}(\mathbf{k}) = 1/\beta \sum_{k_0} D_{\Lambda, \mathbf{q}}^{pp}(k)$ is the non-interacting frequency-summed pair propagator and $B_{\Lambda}^{pp}(\mathbf{q})$ is the p-p bubble in the presence of the cutoff. The factor $1/B_{\Lambda}^{pp}(q)$ has been introduced in such a way, that Eq. (13) acquires a finite limit $\Lambda, \mathbf{q} \rightarrow 0$.

This implies that I^{BCS} has a spectral representation given by

$$I^{BCS}(\mathbf{k}, \mathbf{k}') = \sum_n \lambda_n e_n(\mathbf{k}) e_n(\mathbf{k}'), \quad (14)$$

where λ_n are the eigenvalues of the operator (13) in the limit $\Lambda, \mathbf{q} \rightarrow 0$ and $e_n(\mathbf{k})$ are the corresponding eigenfunctions. The latter satisfy the orthogonality relation

$$\frac{1}{VB_{\Lambda}^{pp}(\mathbf{q})} \sum_{\mathbf{k}} e_n(\mathbf{k}) \tilde{D}_{\Lambda, \mathbf{q}}^{pp}(\mathbf{k}) e_m(\mathbf{k}) = \delta_{nm} \quad (15)$$

in the limit of small \mathbf{q} and Λ .

Using Eqs. (14) and (15), Eq. (10) reduces to a simple geometric series and is easily summed, giving

$$\Gamma_{\Lambda, \mathbf{q}}^{BCS}(\mathbf{k}, \mathbf{k}') = \sum_n \frac{\lambda_n}{1 - \lambda_n B_{\Lambda}^{pp}(\mathbf{q})} e_n(\mathbf{k}) e_n(\mathbf{k}'). \quad (16)$$

³ To be more precise, the operator defined in Eq. (13) is Hermitian with respect to the scalar product given in Eq. (15).

Clearly, positive eigenvalues produce a singularity in the vertex when Λ is lowered to the energy scale Λ_c given by $\lambda_n B_{\Lambda_c}^{pp}(0) = 1$, or equivalently

$$\Lambda_c = W \exp \left(-\frac{1}{\nu(0)\lambda_n} \right). \quad (17)$$

The divergence of the vertex Γ_{Λ}^{BCS} at $\Lambda = \Lambda_c$ is usually interpreted as signaling the onset of superconductivity. In fact, the divergence is caused by low energy p-p pairs and requires some attractive channel in the interaction (corresponding to a positive eigenvalue of I^{BCS}). This suggests that the instability is associated with the formation of Cooper pairs. Moreover formula (17) for the critical energy scale corresponds exactly to the BCS formula for the critical temperature. To establish the connection to BCS-theory, consider the standard gap equation

$$\Delta_{\mathbf{k}} = -\frac{1}{V} \sum_{\mathbf{k}'} g^{BCS}(\mathbf{k}, \mathbf{k}') \frac{\Delta_{\mathbf{k}'}}{2E_{\mathbf{k}'}} \tanh\left(\frac{\beta E_{\mathbf{k}'}}{2}\right), \quad (18)$$

where $g^{BCS}(\mathbf{k}, \mathbf{k}')$ is the coupling function, which describes the scattering of Cooper pairs from momenta \mathbf{k} and $-\mathbf{k}$ towards \mathbf{k}' and $-\mathbf{k}'$. Close to the critical temperature, the mean-field dispersion $E_{\mathbf{k}'} = \sqrt{\Delta_{\mathbf{k}}^2 + \xi_{\mathbf{k}}^2}$ is replaced by $|\xi_{\mathbf{k}}|$. The resulting equation coincides exactly with the eigenvalue equation of the operator (13) at $\mathbf{q} = \mathbf{0}$ and $\Lambda = \Lambda_c$, if we identify $-g^{BCS}(\mathbf{k}, \mathbf{k}')$ with $I^{BCS}(\mathbf{k}, \mathbf{k}')$ and $\Delta_{\mathbf{k}}$, up to a normalizing factor, with $e_n(\mathbf{k})$. We conclude that the eigenfunction $e_n(\mathbf{k})$ with the largest positive eigenvalue determines the momentum-dependence (*s*-wave, *p*-wave, etc.) of the superconducting gap.

It is actually not necessary to calculate the complete function $I^{BCS}(\mathbf{k}, \mathbf{k}')$, but only its value on the Fermi surface. In fact, the eigenvalue equation reduces at small energy scales to

$$\lambda_n e_n(\mathbf{k}) = \frac{1}{V\nu(0)} \sum_{\mathbf{k}'} \delta(\xi_{\mathbf{k}'}) I^{BCS}(\mathbf{k}, \mathbf{k}') e_n(\mathbf{k}') + O\left(\frac{1}{\log \Lambda}\right). \quad (19)$$

Thus, the eigenvalues λ_n and $e_n(\mathbf{k})|_{\xi_{\mathbf{k}}=0}$ are determined by the value of $I^{BCS}(\mathbf{k}, \mathbf{k}')$ on the Fermi surface only. In this sense, the dependence of I^{BCS} on the energies $\xi_{\mathbf{k}}$ and $\xi_{\mathbf{k}'}$ can be classified as irrelevant. The same is true for the dependence on the frequencies k_0 and k'_0 , which has been neglected. Only the dependence on the momenta moving along the Fermi surface is crucial.

4 Superconductivity from repulsive interactions

As an example, we will now calculate the superconducting instabilities for an extended Hubbard model away from half-filling⁴. The electron hopping is restricted to nearest neighbors, i.e. $\xi_{\mathbf{k}} = -2t(\cos k_x + \cos k_y) - \mu$. Fig. 4 shows the Fermi surface for a typical electron density. The variable θ used to parameterize the Fermi surface is defined as the radial angle. The interaction

$$H_I = U \sum_{\mathbf{r}} n_{\uparrow\mathbf{r}} n_{\downarrow\mathbf{r}} + V \sum_{\langle \mathbf{r}, \mathbf{r}' \rangle} n_{\mathbf{r}} n_{\mathbf{r}'} \quad (20)$$

contains a nearest neighbor term V in addition to the Hubbard U . This corresponds to a coupling function $g(\mathbf{k}_1, \mathbf{k}_2, \mathbf{k}_3) = U + 2V[\cos(k_{3,x} - k_{2,x}) + \cos(k_{3,y} - k_{2,y})]$.

We study the superconducting instabilities in two steps. First we calculate within perturbation theory the p-p irreducible vertex $I(\theta, \theta') = I_{\mathbf{q}=0, \Lambda=0}^{BCS}(\mathbf{k}(\theta), \mathbf{k}(\theta'))$, where $\mathbf{k}(\theta)$ is the Fermi momentum corresponding to the angle θ . A discretization of the θ variable into 32 patches is introduced to allow for a

⁴ A similar calculation was performed before by Zanchi and Schulz [ZS96]. Our results are in perfect agreement with theirs.

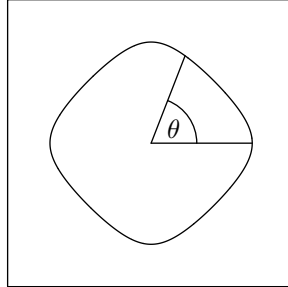


Fig. 4 The Fermi surface of the nearest-neighbor tight-binding band for $\mu = -0.8$ (i.e. $n \approx 0.7$).

numerical treatment. The second step is the solution of the eigenvalue equation (19). This is a trivial numerical operation, once the θ -variable has been discretized.

The eigenfunctions $e_n(\theta)$ can be characterized by their transformation properties with respect to the symmetry group of the square lattice. The D_4 point group has five irreducible representations: A_1, A_2, B_1, B_2 and E . They are illustrated in Table 1.

Irreducible representation	Basis	Simple cases
A_1	$\cos 4m\theta$	s -wave
A_2	$\sin 4m\theta$...
B_1	$\cos(4m+2)\theta$	$d_{x^2-y^2}$
B_2	$\sin(4m+2)\theta$	d_{xy}
E	$\begin{cases} \cos(2m+1)\theta \\ \sin(2m+1)\theta \end{cases}$	p -wave, f -wave

Table 1 Irreducible representations of the D_4 point group, a basis of functions, which span the corresponding subspace (m is an arbitrary integer) and the term commonly assigned to the simplest order parameters in each case. The A_2 subspace consists only of rapidly oscillating functions with at least eight nodes along the Fermi surface.

All the calculations have been done for a repulsive on-site interaction $U = t$. In the case of an attractive $V < 0$, the appearance of superconductivity is not surprising. In fact, the first order vertex $I = -g$ has positive eigenvalues in this case. The results can be seen in Fig. 5. They show triplet p -wave superconductivity for electron densities $n < 0.65$ and singlet $d_{x^2-y^2}$ -wave superconductivity for $0.65 < n$ (close to half filling, additional instabilities arise in the p-h channel). The second order contributions to $I(\theta, \theta')$ give only minor changes to the present result, although they introduce small positive eigenvalues in the symmetry blocks B_2, A_1 and A_2 .

In contrast, in the pure Hubbard model ($V = 0, U > 0$), positive eigenvalues of $I(\theta, \theta')$ appear only via second order terms. Since the sum of three PH2 diagrams is zero in the Hubbard model, the only second order contribution to $I(\theta, \theta')$ comes from the PH1 diagram. The latter is computed numerically, using a mesh of 3000×3000 k-points in the Brillouin zone and a temperature $T = 0.001t$. Kohn and Luttinger have investigated the same diagram in their historical paper [KL65]. The difference is that we are dealing with an anisotropic 2D system as opposed to the isotropic 3D case considered in [KL65].

The results in Fig. 6 for the Hubbard model show d_{xy} -wave symmetry for $n < 0.5$ and $d_{x^2-y^2}$ -wave for $n > 0.6$. In between there is a narrow range of densities where triplet superconductivity (with an f -wave like order parameter) is favored. Note that the eigenvalues of Fig. 6 created by second order terms are in general smaller than those in Fig 5 with an attractive V , leading to a superconductivity at lower energy scales.

The appearance of superconductivity by second-order corrections to the vertex has a physical interpretation in terms of an effective attractive interaction, which is mediated by spin fluctuations. In fact, $I(\theta, \theta')$

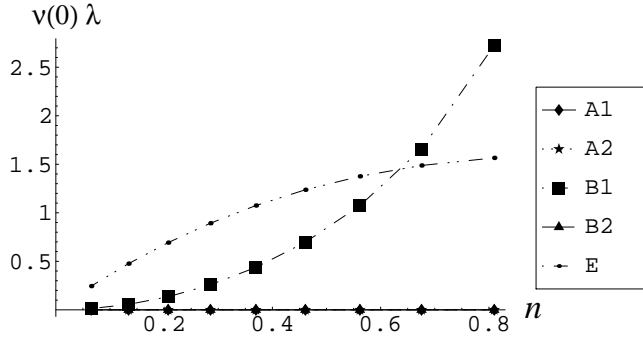


Fig. 5 The positive eigenvalues of $I(\theta, \theta')$ multiplied by the density of states at the Fermi level as a function of the electron density for an attractive nearest-neighbor interaction $V = -0.1t$ and $U = t$, as obtained by a first order calculation. The only positive eigenvalues are in the E and B_1 symmetry block. The corresponding eigenfunctions are p -wave like (for E) and $d_{x^2-y^2}$ -wave like (for B_1). The quantity $v(0)\lambda$ determines the energy scale of the superconducting instability (see Eq. (17)).

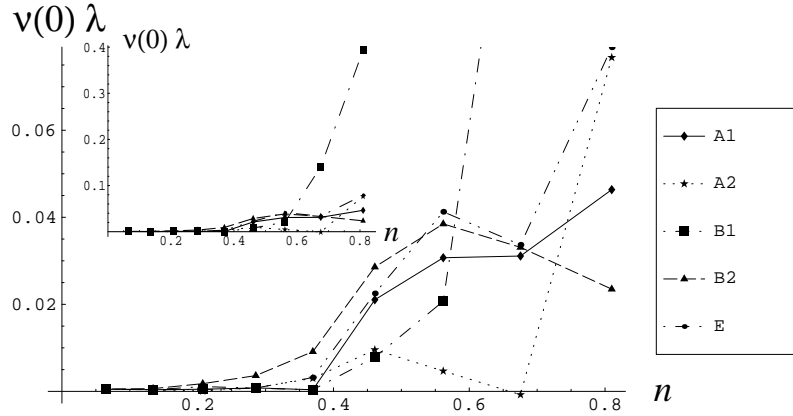


Fig. 6 Same as Fig. 5 from a second order calculation for the pure Hubbard model $V = 0$ and $U = 0.5t$ (Kohn-Luttinger superconductivity). The largest eigenvalue of each symmetry block is shown. The corresponding eigenfunctions are d_{xy} -wave like for B_2 ($n < 0.5$) and $d_{x^2-y^2}$ -wave like for B_1 ($n > 0.6$), and approximately f -wave for E (which is leading only in a narrow range of dopings). The inset shows the global behavior with its drastic increase of the $d_{x^2-y^2}$ -wave eigenvalue close to half-filling.

equals

$$I(\theta, \theta') = -U - U^2 \chi_0(\mathbf{k}_\theta + \mathbf{k}_{\theta'}), \quad (21)$$

where $\chi_0(\mathbf{q})$ is the spin susceptibility of the non-interacting system. The attractive part of $I(\theta, \theta')$ comes therefore from the spin susceptibility $\chi_0(\mathbf{q})$. It is thus fair to say that an effective attraction is created by the exchange of spin fluctuations. The situation is analogous to the conventional superconductivity of metals, where an effective attraction is created through the exchange of phonons, however with the important difference that the same electrons which feel the effective interaction are also responsible for the spin fluctuations.

The idea of spin-fluctuation-induced pairing has led to semi-phenomenological theories of superconducting materials with strong magnetic correlations such as the cuprates which are antiferromagnets in the absence of doping [BSW89, BS89, MTU90, MP92, KM99].

These results strongly support that there is superconductivity in the repulsive Hubbard model at weak coupling. While for electron densities smaller than 0.6 we expect superconductivity only at exponentially small temperatures, the energy scale for $d_{x^2-y^2}$ -pairing increases drastically as the system approaches half-filling. This effect is partly due to the enhanced density of states, but approximate nesting, which enhances spin fluctuations and thus the effective attraction among electrons, is likely to be more important. Very close to half filling, spin fluctuations become so strong that the ladder approximation is no longer valid, and a consistent treatment of both p-p and p-h diagrams is required. This is the subject of the remaining part of this paper.

5 Nesting

In section 3 it was assumed that the divergences in the perturbation series of the vertex are exclusively generated by the p-p diagram. The divergence in the p-p diagram at $\mathbf{k} = 0$ depends on the parity relation $\xi_{\mathbf{p}} = \xi_{-\mathbf{p}}$, which is applicable quite generally.

In contrast, divergences in the p-h diagrams arise only if the Fermi surface has the so-called nesting property. A Fermi surface FS is called p-h nested if the following conditions are satisfied.

1. There exists a vector \mathbf{Q} such that FS has some finite overlap⁵ with its own translation $\mathbf{Q} + FS$.
2. The overlap is such that the occupied part ($\xi_{\mathbf{p}} < 0$) in the vicinity of FS is covering the empty region ($\xi_{\mathbf{p}} > 0$) of $\mathbf{Q} + FS$ and vice versa.

In this case the p-h diagram PH1 shows a logarithmic divergence for $\mathbf{q}_1 = \mathbf{Q}$ and PH2 is divergent for $\mathbf{q}_2 = \mathbf{Q}$. For example every bipartite lattice (i.e. a lattice with electrons hopping only from one sub-lattice A to another sub-lattice B) leads to a p-h nested Fermi surface at half filling.

Similarly one can define p-p nesting as follows.

1. There exists a vector \mathbf{K} such that FS has some finite overlap with $\mathbf{K} - FS$.
2. The overlap is such that the occupied (empty) side of FS is covering the occupied (empty) side of $\mathbf{K} - FS$.

In this case, the p-p diagram PP shows a logarithmic divergence for $\mathbf{k} = \mathbf{K}$. For example, every Fermi surface with spatial inversion symmetry is p-p nested for $\mathbf{K} = 0$.

These are necessary conditions for the occurrence of infrared divergences if the density of states at the Fermi level is finite, i.e. in the absence of van Hove singularities.

The situation is particularly rich if the Fermi surface has flat portions. In this case there is usually a continuum of nesting vectors satisfying the above conditions. RG or parquet calculations for this case are provided in Refs. [ZYD97, VdA01, DVdA02].

6 Bethe-Salpeter equations

If the divergences arise in both p-p and p-h bubbles, the ladder approximation used in section 3 is not sufficient. In fact, in such cases the leading term of the perturbative expansion (8) is given by the so-called parquet diagrams. These diagrams are obtained by retaining the five one-loop (or second order) diagrams

⁵ By “finite overlap”, we mean an overlap with a finite $(D - 1)$ -dimensional volume. Thus a single overlapping point is sufficient for $D = 1$ (and ladder systems), for $D = 2$ it should be a curve of finite length, etc.

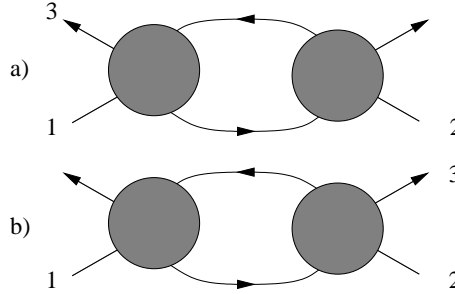


Fig. 7 The structure of diagrams, which are reducible in the p-h 1 channel (a) and the p-h 2 channel (b). The grey circles represent any sub-diagram.

shown in Fig. 1 and by replacing any bare vertex by one of the one-loop diagrams and continuing this process to any order. An example is given in Appendix B.

To keep track of all the logarithmic divergences, one defines three different “channels” of two-particle reducible diagrams. A diagram is called reducible in the p-p channel if it has the structure shown in Fig. 2. Similarly, the diagrams of the form shown in Fig. 7 b) and c) are called reducible in the channels p-h 1 and p-h 2, respectively.

Let us denote by

- $R_{\Lambda}^{pp}(k_1, k_2, k_3)$ the set of reducible diagrams in the p-p channel, with an infrared cutoff Λ ,
- $R_{\Lambda}^{ph1}(k_1, k_2, k_3)$ the set of reducible diagrams in the p-h 1 channel,
- $R_{\Lambda}^{ph2}(k_1, k_2, k_3)$ the set of reducible diagrams in the p-h 2 channel,
- $I_{\Lambda}(k_1, k_2, k_3)$ The set of two particle irreducible diagrams.

It is rather simple to check that a given diagram is either two-particle irreducible or reducible in only one of the three possible channels p-p, p-h 1 and p-h 2. Hence

$$\Gamma_{\Lambda} = I_{\Lambda} + R_{\Lambda}^{pp} + R_{\Lambda}^{ph1} + R_{\Lambda}^{ph2}. \quad (22)$$

The set of irreducible graphs in each of the three channels $\diamond = pp, ph1$ or $ph2$ is defined by $I_{\Lambda}^{\diamond} = \Gamma_{\Lambda} - R_{\Lambda}^{\diamond}$. We already encountered I_{Λ}^{pp} in section 3, where it could be calculated within perturbation theory. This is no longer true in the present case, where infrared divergences occur in the p-h channels as well.

Clearly, R_{Λ}^{pp} is given by the ladder series Eq. (10), but without the first (zero bubble) term. The first-order term is missing since it corresponds to an irreducible contribution. We write this series formally as

$$R_{\Lambda}^{pp} = I_{\Lambda}^{pp} D_{\Lambda}^{pp} I_{\Lambda}^{pp} + I_{\Lambda}^{pp} D_{\Lambda}^{pp} I_{\Lambda}^{pp} D_{\Lambda}^{pp} I_{\Lambda}^{pp} + \dots \quad (23)$$

It satisfies the integral equation

$$R_{\Lambda}^{pp} = I_{\Lambda}^{pp} D_{\Lambda}^{pp} I_{\Lambda}^{pp} + I_{\Lambda}^{pp} D_{\Lambda}^{pp} R_{\Lambda}^{pp} \quad (24)$$

or, using the relation $\Gamma = I^{pp} + R^{pp}$,

$$R_{\Lambda}^{pp} = I_{\Lambda}^{pp} D_{\Lambda}^{pp} \Gamma_{\Lambda}. \quad (25)$$

This is the Bethe-Salpeter equation⁶. With all the functional dependences included it reads

$$R_{\Lambda}^{pp}(k_1, k_2, k_3) = \frac{1}{\beta V} \sum_p I_{\Lambda}^{pp}(k_1, k_2, k-p) D_{\Lambda, k}^{pp}(p) \Gamma_{\Lambda}(p, k-p, k_3), \quad (26)$$

where $k = k_1 + k_2$ and $D_{\Lambda, k}^{pp}(p) = G_{\Lambda}(p)G_{\Lambda}(k-p)$.

⁶ See for example [AGD61, Noz64]. The Bethe-Salpeter equation was originally introduced to calculate two-particle bound-states within quantum electrodynamics [SB51].

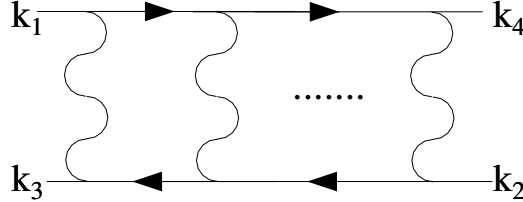


Fig. 8 The p-h ladder diagrams. The wavy stand for $-I_{\Lambda}^{ph1}$ and the electron lines represent full propagators G_{Λ} .

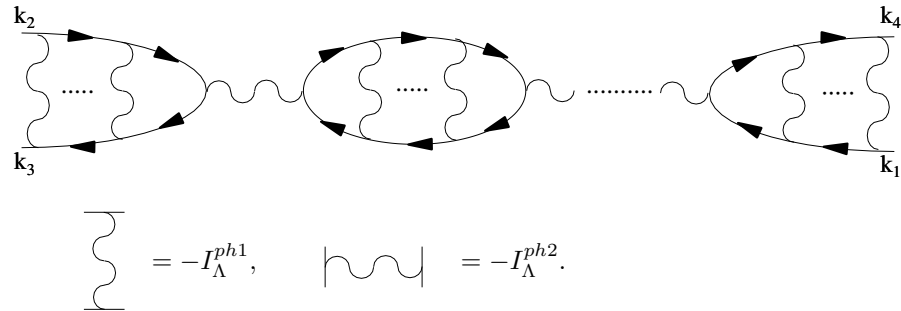


Fig. 9 The general structure of a reducible diagram in the p-h 2 channel. The wavy lines drawn horizontally stand for $-I_{\Lambda}^{ph2}$, but the wavy lines drawn vertically stand for $-I_{\Lambda}^{ph1}$. The electron lines stand for full propagators G_{Λ} .

There are similar equations for the two other channels. First, R_{Λ}^{ph1} is given by a series over the p-h ladders shown in Fig. 8, where the wavy lines stand for $-I_{\Lambda}^{ph1}$ and the electron lines denote the full propagators G_{Λ} . In complete analogy with the p-p case one finds the Bethe-Salpeter equation for the p-h 1 channel

$$R_{\Lambda}^{ph1}(k_1, k_2, k_3) = \frac{1}{\beta V} \sum_p I_{\Lambda}^{ph1}(k_1, p + q_1, k_3) D_{\Lambda, q_1}^{ph}(p) \Gamma_{\Lambda}(p, k_2, p + q_1), \quad (27)$$

where $q_1 = k_3 - k_1$ and

$$D_{\Lambda, q}^{ph}(p) = G_{\Lambda}(p) G_{\Lambda}(p + q). \quad (28)$$

The p-h 2 channel is more involved. In fact, a general R_{Λ}^{ph2} -diagram has the structure shown in Fig. 9, where the wavy lines drawn horizontally stand for $-I_{\Lambda}^{ph2}$, but the wavy lines drawn vertically correspond to $-I_{\Lambda}^{ph1}$. The electron lines stand for full propagators G_{Λ} . Note that the diagram must have at least one horizontal wavy line (in the opposite case it is a p-h ladder and not reducible in the p-h 2 channel).

The simplest examples of p-h 2-reducible diagrams are shown in Fig. 1. The first PH2 diagram of this figure is given by

$$-2 \frac{1}{\beta V} \sum_p I_{\Lambda}^{ph2}(k_1, p, p + q_2) D_{\Lambda, q_2}^{ph}(p) I_{\Lambda}^{ph2}(p + q_2, k_2, k_3), \quad (29)$$

where $q_2 = k_3 - k_2$. We will write this specific convolution of the functions I_{Λ}^{ph2} and D_{Λ}^{ph} as a formal product

$$-2 I_{\Lambda}^{ph2} D_{\Lambda}^{ph} I_{\Lambda}^{ph2}. \quad (30)$$

Note that this notation differs from the formal product introduced before in the p-p case.

With this notation one can write

$$R^{ph2} = -2 I^{ph2} D^{ph} I^{ph2} + (X I^{ph1}) D^{ph} I^{ph2} + I^{ph2} D^{ph} (X I^{ph1}) + \text{"higher order terms,"} \quad (31)$$

where the overall Λ -index has been omitted for the simplicity of notation and $X F(k_1, k_2, k_3) = F(k_2, k_1, k_3)$ for any function of three energy-momenta. The p-h ladder series can also be written using the same notation:

$$X R^{ph1} = (X I^{ph1}) D^{ph} (X I^{ph1}) + \text{"higher order terms."} \quad (32)$$

The following definitions turn out to be very useful.

$$\begin{aligned} R^c &= 2R^{ph2} - X R^{ph1}, \\ I^c &= 2I^{ph2} - X I^{ph1}, \\ \Gamma^c &= I^c + R^c = (2 - X)\Gamma \end{aligned} \quad (33)$$

and

$$\begin{aligned} R^s &= -X R^{ph1}, \\ I^s &= -X I^{ph1} \\ \Gamma^s &= I^s + R^s = -X\Gamma. \end{aligned} \quad (34)$$

The superscripts c and s refer to charge and spin, respectively. Note that $\Gamma^{c/s} = \Gamma^{\uparrow\uparrow} \pm \Gamma^{\uparrow\downarrow}$, so these vertex functions enter naturally in the calculation of charge- and spin- response functions.

Eqs. (31) and (32) can now be written in the simple form

$$R^{s,c} = -I^{s,c} D^{ph} I^{s,c} + \text{"higher order terms."} \quad (35)$$

The exact expressions for $R^{s,c}$ are given by the infinite series

$$R^{s,c} = -I^{s,c} D^{ph} I^{s,c} + I^{s,c} D^{ph} I^{s,c} D^{ph} I^{s,c} - \dots \quad (36)$$

In order to prove Eq. (36), we first write R^{ph2} as an infinite series $R^{ph2} = \sum_{n=1}^{\infty} R_n^{ph2}$, where R_n^{ph2} is the set of diagrams, which are exactly n -times reducible in the p-h 2 channel. A similar decomposition is done for R^{ph1} .

The recursion relations between R_{n+1}^{ph1} , R_{n+1}^{ph2} and R_n^{ph1} , R_n^{ph2} are shown graphically in Figs. 10 and 11. The relation for R_n^{ph2} (Fig. 10) can be understood as follows. A general R_{n+1}^{ph2} -diagram as shown in Fig. 9 can either start on the left with a vertical or a horizontal wavy line. If it starts with a vertical line, then it is given by the second diagram of Fig. 10. If it starts with a horizontal line, there are two cases. If there are no other horizontal lines except for the starting one, the diagram is given by the third term of Fig. 10. If there is more than one horizontal line in the diagram, it is given by the first diagram in Fig. 10.

Analytically the equations depicted in Figs. 10 and 11 read

$$R_{n+1}^{ph2} = -2 I^{ph2} D^{ph} R_n^{ph2} + X I^{ph1} D^{ph} R_n^{ph2} + I^{ph2} D^{ph} X R_n^{ph1} \quad (37)$$

$$X R_{n+1}^{ph1} = X I^{ph1} D^{ph} R_n^{ph1}, \quad (38)$$

or, with the definitions (33) and (34),

$$R_{n+1}^{s,c} = -I^{s,c} D^{ph} R_n^{s,c}. \quad (39)$$

From this, it is easy to deduce Eq. (36).

In analogy to the p-p case, we find now the Bethe-Salpeter equations for Γ^s and Γ^c

$$R^{s,c} = -I^{s,c} D^{ph} \Gamma^{s,c}. \quad (40)$$

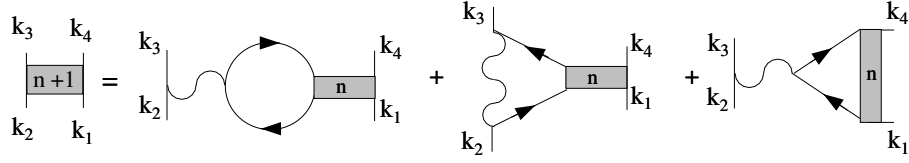


Fig. 10 The recursion relation for R_{n+1}^{ph2} . Wavy lines drawn horizontally stand for I^{ph2} and wavy lines drawn vertically stand for I^{ph1} . The grey rectangles with index n stand for R_n^{ph2} (R_n^{ph1}) if they are drawn horizontally (vertically).

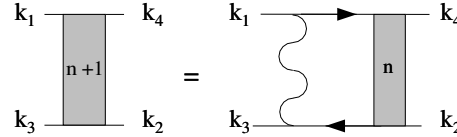


Fig. 11 The recursion relation for R_{n+1}^{ph1} . The conventions are as in Fig. 10

7 RG flow of the vertex

The Bethe-Salpeter equations (26) and (40), three integral equations for the three unknown functions R^{pp} , R^c and R^s , are in general difficult to solve.

We will address the more modest task of calculating the leading term in the perturbative expansion (8). This will be accomplished via the flow equation, i.e. a differential equation for $\partial_\Lambda \Gamma$ where we keep only the leading terms in $\Lambda \rightarrow 0$.

Within this approximation, the two-particle irreducible vertex I is given by the bare interaction $-g$. Thus by Eq. (22),

$$\dot{\Gamma}(k_1, k_2, k_3) = \dot{R}^{pp}(k_1, k_2, k_3) + \dot{R}^{ph1}(k_1, k_2, k_3) + \dot{R}^{ph2}(k_1, k_2, k_3), \quad (41)$$

where the dot means a partial derivative with respect to Λ .

Consider the first term \dot{R}^{pp} . The derivative of the Bethe-Salpeter equation (25) has three contributions

$$\dot{R}^{pp} = \dot{I}^{pp} D^{pp} \Gamma + I^{pp} \dot{D}^{pp} \Gamma + I^{pp} D^{pp} \dot{\Gamma}. \quad (42)$$

Although \dot{I}^{pp} is by no means negligible by itself (since it contains terms which are reducible in the p-h channels), the first contribution, $\dot{I}^{pp} D^{pp} \Gamma$, can be shown to be of subleading order in Λ . We will not prove this here, but an example is discussed in detail in Appendix B. The last term is written as $I^{pp} D^{pp} \dot{I}^{pp} + I^{pp} D^{pp} \dot{R}^{pp}$ and $I^{pp} D^{pp} \dot{I}^{pp}$ is neglected for the same reason as $\dot{I}^{pp} D^{pp} \Gamma$. Therefore

$$\dot{R}^{pp} = I^{pp} \dot{D}^{pp} \Gamma + I^{pp} D^{pp} \dot{R}^{pp}. \quad (43)$$

This equation can be iterated to give

$$\begin{aligned} \dot{R}^{pp} &= I^{pp} \dot{D}^{pp} \Gamma + I^{pp} D^{pp} I^{pp} \dot{D}^{pp} \Gamma + I^{pp} D^{pp} I^{pp} D^{pp} I^{pp} \dot{D}^{pp} \Gamma + \dots \\ &= I^{pp} \dot{D}^{pp} \Gamma + R^{pp} \dot{D}^{pp} \Gamma \\ &= \Gamma \dot{D}^{pp} \Gamma, \end{aligned} \quad (44)$$

or written out with the full functional dependencies

$$\dot{R}_\Lambda^{pp}(k_1, k_2, k_3) = \frac{1}{\beta V} \sum_p \Gamma_\Lambda(k_1, k_2, k - p) \dot{D}_{\Lambda, k}^{pp}(p) \Gamma_\Lambda(p, k - p, k_3), \quad (45)$$

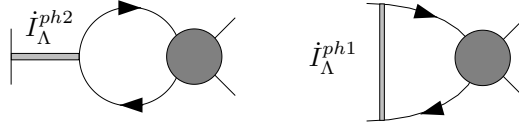


Fig. 12 Negligible terms in the flow equation for $\partial_\Lambda \Gamma$. The grey circles stand for any sub-diagram.

where $k = k_1 + k_2$ is the total frequency-momentum.

The same kind of differential equations are obtained in an analogous way for the p-h channels⁷. Using Eqs. (40) and (36), we obtain

$$\dot{R}^{s,c} = -I^{s,c} \dot{D}^{ph} \Gamma^{s,c} - I^{s,c} D^{ph} \dot{R}^{s,c} \quad (46)$$

$$= -I^{s,c} \dot{D}^{ph} \Gamma^{s,c} + I^{s,c} D^{ph} I^{s,c} \dot{D}^{ph} \Gamma^{s,c} - \dots \quad (47)$$

$$= -I^{s,c} \dot{D}^{ph} \Gamma^{s,c} - R^{s,c} \dot{D}^{ph} \Gamma^{s,c} \quad (48)$$

$$= -\Gamma^{s,c} \dot{D}^{ph} \Gamma^{s,c}. \quad (49)$$

The only point to be verified is that the terms $I^{s,c} D^{ph} \Gamma^{s,c}$ and $I^{s,c} D^{ph} \dot{R}^{s,c}$, which have been left out in Eq. (46), are in fact of subleading order in Λ . Writing out $\dot{R}^{s,c}$ in terms of \dot{R}^{ph1} and \dot{R}^{ph2} , one can verify that all the neglected terms are of the form shown graphically in Fig. 12. They can be shown to be negligible in analogy with the example of Appendix B.

Eq. (49), expressed in terms of R^{ph1} and R^{ph2} leads to

$$\dot{R}^{ph1} = X \left((X\Gamma) \dot{D}^{ph} (X\Gamma) \right) \quad (50)$$

$$\dot{R}^{ph2} = -2\Gamma \dot{D}^{ph} \Gamma + (X\Gamma) \dot{D}^{ph} \Gamma + \Gamma \dot{D}^{ph} (X\Gamma), \quad (51)$$

or written out:

$$\dot{R}_\Lambda^{ph1}(k_1, k_2, k_3) = \frac{1}{\beta V} \sum_p \dot{D}_{\Lambda, q_1}^{ph}(p) \Gamma_\Lambda(p, k_2, p + q_1) \Gamma_\Lambda(k_1, p + q_1, k_3) \quad (52)$$

$$\begin{aligned} \dot{R}_\Lambda^{ph2}(k_1, k_2, k_3) = & \frac{1}{\beta V} \sum_p \dot{D}_{\Lambda, q_2}^{ph}(p) [-2\Gamma_\Lambda(k_1, p, p + q_2) \Gamma_\Lambda(p + q_2, k_2, k_3) \\ & + \Gamma_\Lambda(p, k_1, p + q_2) \Gamma_\Lambda(p + q_2, k_2, k_3) + \Gamma_\Lambda(k_1, p, p + q_2) \Gamma_\Lambda(k_2, p + q_2, k_3)], \end{aligned} \quad (53)$$

where $q_1 = k_3 - k_1$, $q_2 = k_3 - k_2$ are the direct and exchanged transferred momenta and $D_\Lambda^{ph}(p, q) = G_\Lambda(p)G_\Lambda(p + q)$.

Eqs. (41), (45), (52) and (53) are the one-loop RG equations we were looking for. They describe the behavior of the vertex under a differential change of the energy scale Λ . For the sake of clarity, these equations are collected in Table 2 and are referred to as “the one-loop RG equations” in the following.

These equations have a very simple diagrammatic interpretation. The three terms \dot{R}^{pp} , \dot{R}^{ph1} and \dot{R}^{ph2} correspond to the one-loop diagrams shown in Fig. 1, where the wavy lines now represent full vertices Γ_Λ and the product of two single particle propagators has to be derived with respect to Λ . Since $\dot{D}_{\Lambda, q}^{pp/ph}(p) = \dot{G}_\Lambda(p)G_\Lambda(q \pm p) + G_\Lambda(p)\dot{G}_\Lambda(q \pm p)$, each diagram can be viewed as the sum of two terms, where one of the two lines represents the propagator $G_\Lambda(p)$ and the other is $\dot{G}_\Lambda(p)$, the propagator restricted to the energy scale Λ .

⁷ Remember that the formal products of functions mean something different in Eq. (49) than in Eq. (44). The formal product in the p-p channel is defined by Eqs. (25) and (26), whereas the formal product in the p-h channels is defined by Eqs. (29) and (30).

$$\begin{aligned}
\dot{\Gamma}(k_1, k_2, k_3) &= \dot{R}^{pp}(k_1, k_2, k_3) + \dot{R}^{ph1}(k_1, k_2, k_3) + \dot{R}^{ph2}(k_1, k_2, k_3) \\
\dot{R}^{pp}_\Lambda(k_1, k_2, k_3) &= \frac{1}{\beta V} \sum_p \dot{D}_{\Lambda, k}^{pp}(p) \Gamma_\Lambda(k_1, k_2, k - p) \Gamma_\Lambda(p, k - p, k_3) \\
\dot{R}^{ph1}_\Lambda(k_1, k_2, k_3) &= \frac{1}{\beta V} \sum_p \dot{D}_{\Lambda, q_1}^{ph}(p) \Gamma_\Lambda(p, k_2, p + q_1) \Gamma_\Lambda(k_1, p + q_1, k_3) \\
\dot{R}^{ph2}_\Lambda(k_1, k_2, k_3) &= \frac{1}{\beta V} \sum_p \dot{D}_{\Lambda, q_2}^{ph}(p) [-2\Gamma_\Lambda(k_1, p, p + q_2) \Gamma_\Lambda(p + q_2, k_2, k_3) \\
&\quad + \Gamma_\Lambda(p, k_1, p + q_2) \Gamma_\Lambda(p + q_2, k_2, k_3) + \Gamma_\Lambda(k_1, p, p + q_2) \Gamma_\Lambda(k_2, p + q_2, k_3)]
\end{aligned}$$

Table 2 The one-loop RG equations, where $k = k_1 + k_2$ is the total frequency-momentum and $q_1 = k_3 - k_1$, $q_2 = k_3 - k_2$ are the direct and exchanged transferred frequency-momenta, respectively. The p-p and p-h propagators are defined as $D_{\Lambda, k}^{pp}(p) = G_\Lambda(p)G_\Lambda(k - p)$ and $D_{\Lambda, q}^{ph}(p) = G_\Lambda(p)G_\Lambda(p + q)$.

Although we have defined Λ as a sharp infrared cutoff in the band energy, the RG equations are also correct for a cutoff in the frequency or for smooth cutoffs. It is straightforward to use the finite temperature instead of a cutoff to regularize the theory. The RG equations for $\partial_T \Gamma_T$ are then obtained by replacing in Table 2

$$\frac{1}{\beta V} \sum_p \dot{D}^\diamond(p, q) \dots \rightarrow \frac{1}{V} \sum_{n \in \mathbf{Z}, \mathbf{p}} \partial_T \left(\frac{1}{\beta} D^\diamond(p, q) \Big|_{p_0=2\pi T(2n+1)} \right) \dots, \quad (54)$$

where $\diamond = pp, ph$.

Different regularizations of the theory give the same result to leading logarithmic order. For instance, the vertex at zero temperature and finite infrared cutoff Λ is, within logarithmic precision, equal to the vertex at temperature $T = \Lambda$ without cutoff.

Let us close this section with the remark that the present RG formalism allows the calculation, to leading order in the infrared cutoff, of various generalized susceptibilities, i.e. the linear response of the system to weak external perturbations. The required relations are derived in Appendix C.

8 Discussion of the low-energy behavior

The leading terms for $\Lambda \rightarrow 0$ of the right-hand side of the one-loop RG equations behave like $\sim \Gamma_\Lambda^2 \Lambda^{-1}$ (note that Λ^{-1} is the derivative of the logarithm). However, the one-loop RG equations contain in general many non-leading terms, like \dot{R}_Λ^{pp} if \mathbf{k} is not a p-p nesting vector and \dot{R}_Λ^{ph1} if \mathbf{q}_1 is not a p-h nesting vector, etc. These terms are diverging at most as $\sim \Gamma_\Lambda^2 \log \Lambda$.

Since the one-loop RG equations are only correct to leading order in Λ , only the leading terms are to be taken seriously. Taking into account subleading terms in the one-loop RG equations is inconsistent and arbitrary, since these subleading terms are comparable to terms that have been neglected. The contributions to the exact RG flow can be classified into three classes: 1. leading terms of the one-loop equation, 2. subleading terms of the one-loop equation and 3. terms which are neglected in the one-loop equation. One has to compare the subleading terms $\sim \Gamma_\Lambda^2 \log \Lambda$ with the neglected terms. According to a careful analysis by Salmhofer and Honerkamp [SH01], the first neglected terms are of the order $\sim \Gamma_\Lambda^3 \log^2 \Lambda$ (see Eq. 108

of [SH01]). Schematically,

$$\dot{\Gamma}_\Lambda = \underbrace{\text{“leading terms”}}_{\sim \Gamma_\Lambda^2 \Lambda^{-1}} + \underbrace{\text{“subleading terms”}}_{\sim \Gamma_\Lambda^2 \log \Lambda} + \underbrace{\text{“neglected terms”}}_{\sim \Gamma_\Lambda^3 \log^2 \Lambda}. \quad (55)$$

The RG flow is split into three different energy regimes.

1. **High energies**, in which Λ is not small. In this regime, the subleading terms of the one-loop equation dominate the neglected two-loop terms, provided $\Gamma_\Lambda \log \Lambda$ is small. Thus the one-loop RG equations can in principle be used to calculate Γ_Λ , starting with a cutoff equal to the bandwidth, where the vertex is given by the bare coupling. In this regime, there is no small parameter to further simplify the functional RG equations, so using them is technically very difficult. But in the high energy regime ($g \log \Lambda \ll 1$) naïve perturbation theory provides a controlled and much more feasible method of calculation than the RG.
2. **Small energies**, where Λ is small such that $(\Lambda \log \Lambda)^{-1} \gg \Gamma_\Lambda \log \Lambda \sim 1$. Naïve perturbation theory breaks down in this regime, but the leading terms of the one-loop RG equations are superior to the neglected terms even if Γ is not necessarily small. This is where the one-loop RG is most useful. Note, that the subleading terms are no longer superior to the neglected terms in this regime. Thus, they have also to be neglected to be consistent. The small parameter Λ justifies to replace every vertex $\Gamma(k_1, k_2, k_3)$ in the one-loop RG equations by its value on the Fermi surface ($k_{0,1} = k_{0,2} = k_{0,3} = \xi_{\mathbf{k}_1} = \xi_{\mathbf{k}_2} = \xi_{\mathbf{k}_3} = 0$), for reasons given in the end of section 3 (for the case where the instabilities only occur in the p-p channel) and in Appendix B (for the nested case).
3. **The critical regime**, where Λ is close to the critical energy scale Λ_c at which Γ_Λ is diverging. If Λ is too close to Λ_c , the neglected terms are no longer negligible and the one-loop approximation is no longer accurate. Note however that the weaker the initial interaction is, the more Λ can approach Λ_c before the one-loop approximation breaks down.

This remark about subleading terms concerns in particular the self-energy corrections to the propagator G_Λ . As already pointed out after Eq. (10), the self-energy changes the shape and location of the Fermi surface. This effect is by no means negligible in perturbation theory. Other effects, such as the renormalization of the Fermi velocity or the reduction of the quasi-particle weight are of subleading order. So these effects cannot be taken into account consistently within the one-loop approximation. For this reason, it is a consistent approximation to replace the dressed electron propagators G_Λ in the one-loop RG equations by the bare ones C_Λ .

9 Relation to the Wilsonian approach

A key ingredient to the Wilsonian RG is the idea to replace the given problem by a different one with less degrees of freedom but with the same low energy behavior. To achieve this, the effect of the eliminated degrees of freedom is incorporated in a renormalization of the parameters of the effective low-energy theory.

This strategy has been successfully followed using Brillouin-Wigner perturbation theory in the strong coupling limit of various many-body problems (see for example [Eme79, Aue94, Faz99]). The best known example is the Hubbard model at half-filling which is represented, in the limit of strong coupling, by a Heisenberg spin Hamiltonian in the limit of strong coupling.

In the weak coupling limit, the application of the Brillouin-Wigner formalism to compute an effective Hamiltonian is less evident and has not been followed to our knowledge. A tractable implementation of the same idea (i.e. elimination of high energy degrees of freedom and renormalization of parameters of the effective theory) is given more easily in the functional integral representation.

It should nevertheless be mentioned that the idea of effective Hamiltonians on a reduced Hilbert space led to a most powerful numerical tool for one-dimensional systems: the density matrix renormalization group (see [NW99] for an introduction). An alternative route to effective Hamiltonians was presented recently by Wegner [Weg94] and applied to the 2D Hubbard model [HW03] and other correlated systems [Keh01, HU02].

Some basic definitions and results of the functional integral formalism are given in Appendix D, for a detailed presentation, see [NO88].

The bare propagator is now endowed with an infrared cutoff Λ on the band energy $C_\Lambda(k) = \Theta(|\xi_k| - \Lambda)C(k)$.

The *effective interaction* depending on the energy scale Λ is defined as

$$\mathcal{W}_\Lambda[\chi] = -\log \int d\mu_{C_\Lambda}[\psi] e^{-W[\psi+\chi]}, \quad (56)$$

where $d\mu_{C_\Lambda}[\psi]$ is the normalized Gaussian measure according to the propagator C_Λ (Eq. (129)), and W is the model interaction in terms of Grassmann variables Eq. (123). Note that the integration with respect to $d\mu_{C_\Lambda}[\psi]$ is perfectly defined, although C_Λ^{-1} is not. This can be seen most easily in the expansion of $\mathcal{W}_\Lambda[\chi]$ in terms of Feynman diagrams. The evaluation of these diagrams involves only C_Λ and never C_Λ^{-1} . Whenever C_Λ^{-1} appears in an intermediate step of a calculation, it may be regularized by replacing the zero in the Heavyside function by an infinitesimal number.

The effective interaction $\mathcal{W}_\Lambda[\chi]$, which depends on the Grassmann field χ , has a twofold interpretation. On the one hand, we can restrict the field χ to the low energy degrees of freedom $\psi_{< k\sigma} = \Theta(\Lambda - |\xi_k|)\psi_{k\sigma}$. The object

$$S_\Lambda^{\text{eff}}[\psi_{<}] = (\bar{\psi}_{<}, C^{-1}\psi_{<}) - \mathcal{W}_\Lambda[\psi_{<}] \quad (57)$$

corresponds then to Wilson's effective action, which describes the system in terms of $\psi^{<}$ only. In fact, for observables (or Green's functions) which depend only on the low energy fields, one shows

$$\langle O[\psi^{<}] \rangle = \frac{1}{Z} \int \mathcal{D}\psi^{<} \int \mathcal{D}\psi^{>} e^{S[\psi^{<}, \psi^{>}]} O[\psi^{<}] \quad (58)$$

$$= \frac{1}{Z} \int \mathcal{D}\psi^{<} e^{S_\Lambda^{\text{eff}}[\psi^{<}]} O[\psi^{<}] \quad (59)$$

and

$$Z = \int \mathcal{D}\psi^{<} \int \mathcal{D}\psi^{>} e^{S[\psi^{<}, \psi^{>}]} = \int \mathcal{D}\psi^{<} e^{S_\Lambda^{\text{eff}}[\psi^{<}]} \quad (60)$$

On the other hand, \mathcal{W}_Λ is the generating functional of amputated connected correlation functions with infrared cutoff Λ because of the identity

$$\log Z_\Lambda[\eta] = -(\bar{\eta}, C_\Lambda\eta) - \mathcal{W}_\Lambda[C_\Lambda\eta], \quad (61)$$

where Z_Λ is given by Eq. (128), with C replaced by C_Λ . To prove Eq. (61), we write out the Gaussian measure in (Eq. (129)) explicitly. Then, only in the numerator, we perform a shift of the integration variables $\psi \rightarrow \psi - \chi$. Eq. (61) follows finally by putting $\chi = C_\Lambda\eta$ and taking the logarithm.

As a consequence of Eq. (61), the quadratic part of \mathcal{W}_Λ is related to the self-energy Σ_Λ by

$$\frac{\delta^2}{\delta \chi_{\sigma k} \delta \bar{\chi}_{\sigma k}} \mathcal{W}_\Lambda[\chi] \Big|_{\chi=0} = -C_\Lambda^{-1}(k) - \langle \psi_{\sigma k} \bar{\psi}_{\sigma k} \rangle_\Lambda C_\Lambda^{-2}(k) \quad (62)$$

$$= \frac{\Sigma_\Lambda(k)}{1 - C_\Lambda(k)\Sigma_\Lambda(k)}, \quad (63)$$

where we have used the following identity for the full electron propagator $G_\Lambda(k) = -\langle \psi_{\sigma k} \bar{\psi}_{\sigma k} \rangle_\Lambda = C_\Lambda(k)(1 - C_\Lambda(k)\Sigma_\Lambda(k))^{-1}$. Therefore in the case $|\xi_{\mathbf{k}}| < \Lambda$ the right-hand side of Eq. (63) simply becomes $\Sigma_\Lambda(k)$.

Similarly the quartic part of \mathcal{W}_Λ is related to the one particle irreducible vertex Γ_Λ . In fact, differentiating Eq. (61) we find

$$\frac{\delta^4 \mathcal{W}_\Lambda[\chi]}{\delta \chi_{\sigma k_4} \delta \chi_{\sigma' k_3} \delta \bar{\chi}_{\sigma' k_2} \delta \bar{\chi}_{\sigma k_1}} \Big|_{\chi=0} = -\langle \psi_{\sigma k_1} \psi_{\sigma' k_2} \bar{\psi}_{\sigma' k_3} \bar{\psi}_{\sigma k_4} \rangle_{c, \Lambda} \prod_{i=1}^4 C_\Lambda^{-1}(k_i) \quad (64)$$

$$= -\frac{\Gamma_\Lambda^{\sigma\sigma'}(k_1, \dots, k_4)}{\beta V \prod_{i=1}^4 [1 - C_\Lambda(k_i)\Sigma_\Lambda(k_i)]}. \quad (65)$$

In the last line we have used Eq. (126) and the definition of the vertex (Eq. (77)).

The quartic part of \mathcal{W}_Λ is of the same form as Eq. (123) with an effective coupling function $g_\Lambda(k_1, k_2, k_3)$ that now depends on the frequencies as well as the momenta. Taking functional derivatives of Eq. (123), we find for $|\xi_{\mathbf{k}_i}| < \Lambda$,

$$(1 - \delta_{\sigma\sigma'} X)g_\Lambda(k_1, k_2, k_3) = -\Gamma_\Lambda^{\sigma\sigma'}(k_1, k_2, k_3) \quad (66)$$

and thus

$$g_\Lambda(k_1, k_2, k_3) = -\Gamma_\Lambda(k_1, k_2, k_3). \quad (67)$$

g_Λ is equal, up to the sign, to a connected amputated correlation function if all $|\xi_{\mathbf{k}_i}| > \Lambda$ and to the one-particle irreducible vertex in the opposite case. g_Λ is therefore not continuous at $|\xi_{\mathbf{k}_i}| = \Lambda$. A formal and non-perturbative proof of these relations was given by Morris [Mor94] for a bosonic field theory. The derivation given above is perturbative, but a generalization of the non-perturbative proof of Morris to fermions appears to be straightforward. Morris has also shown that Σ_Λ and Γ_Λ are continuous at $|\xi_{\mathbf{k}_i}| = \Lambda$, in contrast to g_Λ .

10 Other one-loop RG equations

The effective interaction satisfies the following exact RG equation for $\partial_\Lambda \mathcal{W}_\Lambda = \dot{\mathcal{W}}_\Lambda$

$$\dot{\mathcal{W}}_\Lambda[\chi] = \sum_{\sigma, k} \dot{C}_\Lambda(k) \frac{\delta^2 \mathcal{W}_\Lambda[\chi]}{\delta \chi_{\sigma k} \delta \bar{\chi}_{\sigma k}} - \sum_{\sigma, k} \dot{C}_\Lambda(k) \frac{\delta \mathcal{W}_\Lambda[\chi]}{\delta \chi_{\sigma k}} \frac{\delta \mathcal{W}_\Lambda[\chi]}{\delta \bar{\chi}_{\sigma k}}. \quad (68)$$

This equation was first derived by Polchinski in the context of a scalar field theory [Pol84]. Zanchi and Schulz [Zan96, ZS00] proposed to develop \mathcal{W}_Λ up to order six in the fermionic variables and to neglect terms of higher order. Terms of order six are not present in the original interaction but they are produced by the RG procedure. Their effect is then to renormalize the effective coupling function g_Λ . The result is a closed one-loop equation for the coupling function $g_\Lambda(k_1, \dots, k_4)$ where $|\xi_{\mathbf{k}_i}| < \Lambda$. It is identical, within the correspondence $g_\Lambda = -\Gamma_\Lambda$, to our one-loop RG equations in Table 2 with one difference. In the RG equation of Zanchi and Schulz, the vertices on the right hand-side are not evaluated at the scale Λ , but at a higher scale $\tilde{\Lambda}$, which is given by the band energy of the single-particle propagators, i.e. $\tilde{\Lambda} = \text{Max}\{|\xi_{\mathbf{p}}|, |\xi_{\mathbf{k}-\mathbf{p}}|\}$ in the p-p term of Table 2, $\tilde{\Lambda} = \text{Max}\{|\xi_{\mathbf{p}}|, |\xi_{\mathbf{p}+\mathbf{q}_1}|\}$ in the p-h 1 term and $\tilde{\Lambda} = \text{Max}\{|\xi_{\mathbf{p}}|, |\xi_{\mathbf{p}+\mathbf{q}_2}|\}$ in the p-h 2 term. Their equation is thus non-local in Λ . It is a flow equation with memory, i.e. the flow at scale Λ doesn't only depend on the vertex function Γ_Λ but also on the history of the flow.

Since this is not very convenient, it was proposed [HM00] to develop Eq. (68) into Wick ordered polynomials of the fermionic variables instead of monomials as it was done above. Wick ordering with respect to the low energy propagator $D_\Lambda = C - C_\Lambda$ results in the same one-loop equation as above but now all the couplings are evaluated at the actual RG variable Λ and $-d [C_\Lambda(p)C_\Lambda(q)] / d\Lambda$ has to be replaced by $d [D_\Lambda(p)D_\Lambda(q)] / d\Lambda$, i.e., one propagator is at the energy Λ and the energy of the second propagator is now restricted to be *smaller* than Λ . This is different from our one-loop RG equation, where the second propagator is restricted to higher energies.

We have seen above that the coupling function of the low-energy effective theory equals, up to a sign, the one-particle irreducible vertex Γ_Λ . This correspondence can not be generalized to higher order vertices, i.e. it would be completely wrong to say that the sixth order term of \mathcal{W}_Λ is related to the one-particle irreducible part of the three particle Green's function and so forth. In addition, the correspondence Eq. (67) relies on the choice of the cutoff which ensures that $C_\Lambda(p) = 0$, for $|\xi_p| < \Lambda$. The correspondence no longer holds for an alternative scheme, where for example the finite temperature is used to regularize the theory instead of the infrared cutoff.

The general one-particle irreducible vertices are obtained by performing a Legendre transformation on the functional \mathcal{W}_Λ . Wetterich has presented a renormalization group scheme for bosonic field theories, working with this Legendre transformed quantity rather than with the effective action defined in Eq. (56) [Wet93, TW94]. The idea was implemented recently for the many-fermion problem in [HSFR01, SH01]. The resulting RG equation is identical to the one in Table 2 apart from self-energy terms which should be, as we argued above, neglected for consistency reasons. In fact, if the cutoff is introduced by some function multiplying the bare propagator

$$C_\Lambda(p) = \frac{\theta_\Lambda(p)}{ip_0 - \xi_p}, \quad (69)$$

then the full propagator is given by

$$G_\Lambda(p) = \frac{C_\Lambda(p)}{1 - C_\Lambda(p)\Sigma_\Lambda(p)}, \quad (70)$$

$$= \frac{\theta_\Lambda(p)}{ip_0 - \xi_p - \theta_\Lambda(p)\Sigma_\Lambda(p)}. \quad (71)$$

The derivative with respect to Λ gives

$$\dot{G}_\Lambda(p) = \frac{\dot{\theta}_\Lambda(p)(ip_0 - \xi_p)}{(ip_0 - \xi_p - \theta_\Lambda(p)\Sigma_\Lambda(p))^2} + \frac{\theta_\Lambda^2(p)\dot{\Sigma}_\Lambda(p)}{(ip_0 - \xi_p - \theta_\Lambda(p)\Sigma_\Lambda(p))^2}. \quad (72)$$

The first term of the right hand-side is the single-scale propagator of Ref. [HSFR01]. The one-loop RG equations of Salmhofer and Honerkamp are obtained from those in Table 2 by omitting the second term of Eq. (72).

The RG equations of the three groups [ZS00, HM00, HSFR01] differ in the treatment of the diagrams which give not a leading order contribution in the limit $\Lambda \rightarrow 0$. For example, the (leading order) p-p diagram at total momentum $k = 0$ features two internal propagators with exactly opposite momenta. They have exactly the same band energy. So the non-locality of the Zanchi-Schulz equation is not present in this diagram. For the same reason, the energy-constraint of the Wick-ordered scheme can not have any effect in this case. So the three RG schemes treat such diagrams identically. The same is true for the p-h diagrams in the case of perfect nesting. However, as we have argued in section 7, only the leading order terms of these RG equations make sense. The subleading terms are of the same order as others that have been neglected. In fact, a consistent treatment of subleading terms requires going beyond the one-loop approximation.

The equivalence of the different RG equations to leading order can also be understood in the following way. By successively integrating the one-loop RG equations (Table 2) and expressing the result in terms of

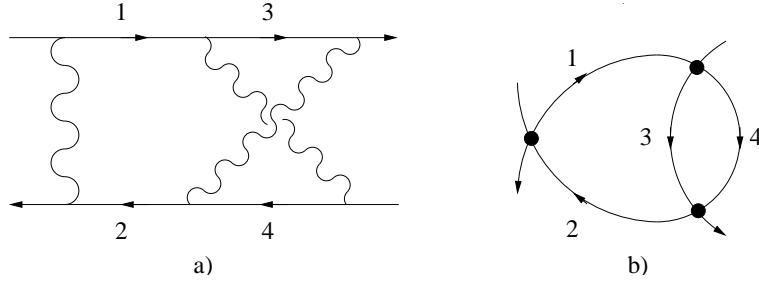


Fig. 13 Fig. a) shows an example of a two loop parquet diagram, where the internal electron propagators are numbered from 1 to 4. Fig. b) shows the same diagram, but the wavy interaction lines are contracted to points in order to make the loop structure more transparent.

$\Gamma_{\Lambda_0} \approx -g$, one obtains the full series of parquet diagrams. However the structure of these RG equations introduces a constraint on the energies of internal lines. For example the parquet diagram of Fig. 13 is generated by the one-loop RG with the following constraint on the propagators 1,2,3 and 4

$$\text{Min}\{|\xi_1|, |\xi_2|\} \leq \text{Min}\{|\xi_3|, |\xi_4|\}. \quad (73)$$

Higher order parquet diagrams are generated with similar constraints, i.e. with a certain “ordering” of the band energies, when one goes from the inner loops to the exterior loops of a given parquet diagram. It can be checked by introducing this constraint into Eq. (85) of Appendix B, that the constraint does not change the value of the diagram to leading logarithmic order in Λ .

The different RG equations [ZS00, HM00, HSR01] all generate the whole series of parquet diagrams, but the constraints are different. In the Wick ordered scheme, the constraint (73) is changed into

$$\text{Max}\{|\xi_1|, |\xi_2|\} \leq \text{Max}\{|\xi_3|, |\xi_4|\}.$$

The RG equation of Zanchi and Schulz introduces the most restrictive constraint

$$\text{Max}\{|\xi_1|, |\xi_2|\} \leq \text{Min}\{|\xi_3|, |\xi_4|\},$$

i.e. both propagators of the inner loop are higher in energy than both propagators of the exterior loop. All these constraints are irrelevant for the leading logarithmic order in Λ . We conclude that our one-loop RG equations and those of Refs. [ZS00, HM00, HSR01] are all equivalent to leading order in Λ .

11 Conclusion

In conclusion, we have presented the RG method of weakly interacting electrons to leading (one-loop) order using a simple framework. We have chosen the point of view of partial summations of the perturbation series, taking into account the leading infrared-diverging terms and neglecting subleading contributions in an unbiased and consistent way. The procedure is controlled by two small parameters, the bare interaction strength and the energy scale of interest.

In the case of a generic Fermi surface in more than one dimension, this procedure leads to the ladder approximation. Our calculations for the two-dimensional Hubbard model away from half filling show a pole in the scattering vertex $\Gamma(p_1, p_2, p_3)$ at $p_1 + p_2 = 0$, where $p_{1,2}$ are the frequency-momenta of the incoming particles. The standard interpretation of this pole is the development of a two-particle bound state, i.e. of a pairing instability. The symmetry of the pairing state is d -wave. The pairing mechanism can be interpreted in terms of an effective attraction between electrons which is created by spin fluctuations. The critical energy scale at which the pole is created increases drastically as half-filling is approached. The

reasons are twofold. First, antiferromagnetic spin fluctuations are enhanced due to approximate nesting and second, the density of states increases due to the proximity of a Van Hove singularity.

However, if the Fermi surface is nested, the summation of p-p ladder diagrams is no longer sufficient, but the more general RG formalism involving p-h as well as p-p contributions is required. As opposed to some more modern formulations [Sha94, ZS00, HM00, HSR01], we have derived the one-loop RG equations by identifying the leading logarithmic terms. We feel that the less modern route chosen here makes the meaning of the one-loop approximation more transparent. In particular, it gives a natural guideline for deciding which terms are to be included in the calculation and which ones are to be neglected for reasons of consistency. For example, we argue in section 8 that if the Fermi surface is not nested and the Fermi level is not close to a Van Hove singularity, the one-loop RG is not better than the ladder approximation. This is also true in the presence of Umklapp scattering, in contrast to the assertions of Ref. [HSFR01]. Furthermore, in section 10, we compare three different versions of RG equations, which were discussed in the literature. We find that all of these approaches are equivalent within the regime of applicability of the one-loop approximation.

The RG approach is most useful in one dimension, or in the case of a flat Fermi surface with many nesting vectors (see section 5 for a precise definition). If there is only one single nesting vector, the situation is simpler. Consider for example an anisotropic square lattice at half filling. The dispersion is given by $\xi_{\mathbf{k}} = -2(t_x \cos k_x + t_y \cos k_y)$, where $0 < |t_y/t_x| < 1$ (not too close to neither 0 or 1). Because the Fermi surface is perfectly nested by (π, π) , there are infrared singularities in the p-h as well as in the p-p channel. However, the non-ladder parquet diagrams appear not to be of the leading order in this case. As a consequence one can just sum the p-h1, p-h2 and p-p ladders separately. In other words, the one-loop RG equations decouple (to leading order) into three different sets, related to pairing-, spin- and charge instabilities, respectively [Bin02]. The study of the p-h instabilities is then in perfect analogy to our treatment of superconductivity in Sections 3 and 4. A repulsive Hubbard-like interaction will lead to a spin-density wave instability.

More difficult and also more interesting is the case, where the Fermi surface passes through saddle points of the dispersion relation. Because the dispersion is quadratic rather than linear at the saddle points, they render infrared divergences more dangerous, particularly in two dimensions, where saddle points lead to a logarithmic Van Hove singularity in the density of states.

We have recently studied the half-filled nearest-neighbor tight-binding band on a square lattice (i.e. the case mentioned above, but with $t_x = t_y$), where the Fermi surface is a perfect square and contains two saddle points. Our investigation yields a rich phase diagram as a function of the model interaction [BBD02]. Apart from s - and $d_{x^2-y^2}$ -wave superconductivity, spin- and charge-density waves as well as two phases with circulating charge or spin currents (d -density waves) appear as possible instabilities. Unlike numerical studies of the functional RG equations [ZS00, HM00, Hon01] which rely on a discretization, we do not obtain a simultaneous divergence of different, say superconducting and spin-density wave susceptibilities as the energy scale is lowered, but only of the leading susceptibility. Although there is no decoupling of the RG equations into independent sets, it turns out that the leading channel asymptotically decouples from the others as an instability is approached [BBD02].

The case of the half-filled nearest-neighbor tight-binding band is special because it features perfect nesting and saddle points at the same time. Considerable effort has been spent on the more general case of a Fermi surface which is at Van Hove filling but not nested. This case is particularly interesting because it potentially contains new physics such as non Fermi liquid behavior [Dzy96, IK01], itinerant ferromagnetism [IKK01, HS01b] or Pomeranchuk instabilities [HM01]. Unfortunately, the one-loop RG equations are likely to be unreliable in this case. The reason is that the one-loop equation generates a correct summation merely of the *leading* divergent terms in the perturbation series, but the above-mentioned phenomena depend on *subleading* logarithmic divergences. This can be seen by considering the following example. To study the ferromagnetic (Stoner) instability, we have to calculate the scattering vertex $\Gamma(k_1, k_2, k_3)$ for an infinitely small momentum transfer, $\mathbf{k}_3 - \mathbf{k}_1 \rightarrow \mathbf{0}$. The instability is usually created by p-h ladder

diagrams (Fig. 8). In the case of Van Hove filling, the zero-momentum limit of the p-h bubble⁸ diverges as $\sim \log T$ for low temperatures⁹ as a consequence of the infinite density of states. This is a subleading divergence compared to the behavior of the zero-momentum p-p bubble, which is $\sim \log^2 T$ in the case of Van Hove filling. The third-order diagram of the p-h ladder series behaves as $U^3 \log^2 T$ since it contains two low-momentum p-h bubbles, each contributing with one logarithm. The one-loop RG theory in addition generates parquet diagrams, where p-p and p-h bubbles are mixed. The diagram shown in Fig. 13 contains one p-h bubble and one (internal) p-p bubble. If the external legs are chosen close to the saddle points, its leading behavior is $U^3 \log^3 T$. The error from the one-loop approximation is of subleading logarithmic order, i.e. in our case of the order $U^3 \log^2 T$. The problem is obviously that the error produced by the one-loop approximation is of the same order as the term which produces the ferromagnetic instability. The difficulty is not only encountered for third-order diagrams but proliferates to every order in perturbation theory. We conclude that the one-loop RG is an uncontrolled approximation for discussing ferromagnetism.

A consistent weak-coupling treatment should at least include a self-consistent determination of the Fermi surface, self-energy corrections to both the quasi-particle weight and the Fermi velocity as well as two-loop corrections to the RG equations of the vertex. Although some progress has already been made on certain of these aspects [Zan01, HS03, NM03], a satisfactory control of the Van Hove case has not yet been obtained. New techniques will have to be developed to settle these issues.

Acknowledgements B. B. thanks N. Dupuis, A. Ferraz, F. Gebhard, F. Guinea, G. I. Japaridze, A. P. Kampf, A. A. Katanin, W. Metzner, T. M. Rice, V. Rivasseau, A. Rosch, B. Roulet, M. Salmhofer, G. S. Uhrig, F. Vistulo de Abreu, D. Vollhardt, M. A. H. Vozmediano and D. Zanchi for useful and stimulating discussions. This work was supported by the Swiss National Foundation through grant no. 20-61470.00, the National Centre of Competence in Research MaNEP (Materials with Novel Electronic Properties) and the Rectors' Conference of the Swiss Universities via a special mobility grant.

A Definition and properties of the vertex function

In this appendix, we give the definition of the imaginary-time two-particle Green's function and the vertex function. These quantities are not directly observable but they are analytically related to various physical response functions [AGD61, FW71, NO88].

The two-particle Green's function is defined as

$$G^{\sigma\sigma'}(\tau_1, \tau_2, \tau_3, \mathbf{k}_1, \mathbf{k}_2, \mathbf{k}_3) = V \langle T c_{\sigma\mathbf{k}_1}(\tau_1) c_{\sigma'\mathbf{k}_2}(\tau_2) c_{\sigma'\mathbf{k}_3}^\dagger(\tau_3) c_{\sigma\mathbf{k}_1+\mathbf{k}_2-\mathbf{k}_3}^\dagger(0) \rangle \quad (74)$$

where V is the system volume (i.e. the number of lattice sites) and T is the time ordering operator. The imaginary time dependence of any operator is given by

$$O(\tau) = e^{\tau(H-\mu N)} O e^{-\tau(H-\mu N)}, \quad (75)$$

where μ is the chemical potential and $N = \sum_{\mathbf{k}\sigma} c_{\mathbf{k}\sigma}^\dagger c_{\mathbf{k}\sigma}$ the particle number operator. The Fourier transform with respect to the τ variables,

$$G^{\sigma\sigma'}(k_1, k_2, k_3) = \int_0^\beta d\tau_1 d\tau_2 d\tau_3 e^{i(k_{01}\tau_1 + k_{02}\tau_2 - k_{03}\tau_3)} G^{\sigma\sigma'}(\tau_1, \tau_2, \tau_3, \mathbf{k}_1, \mathbf{k}_2, \mathbf{k}_3), \quad (76)$$

⁸ The p-h bubble is defined by $B^{ph}(q) = 1/(\beta V) \sum_p C(p)C(p+q)$ and is equal up to the sign to the non-interacting spin susceptibility.

⁹ It is not possible to study long-wavelength p-h response in the presence of an infrared momentum cutoff. The regularization has therefore to be done in another way, for example by a finite temperature.

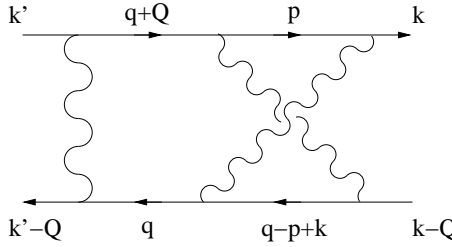


Fig. 14 Example of a two loop parquet diagram.

is a function of the $2 + 1$ -dimensional frequency-momentum vectors $k_i = (k_{0i}, \mathbf{k}_i)$. The Matsubara frequencies k_{0i} run over the odd multiples of π/β , because $G^{\sigma\sigma'}$ is anti-periodic with period β in each of the τ variables.

The vertex function $\Gamma^{\sigma\sigma'}(k_1, k_2, k_3)$, defined as the one-particle irreducible part of $G^{\sigma\sigma'}(k_1, k_2, k_3)$, satisfies the relation

$$G^{\sigma\sigma'}(k_1, k_2, k_3) = \beta V(\delta_{k_2, k_3} - \delta_{\sigma, \sigma'} \delta_{k_1, k_3}) G(k_1) G(k_2) + \Gamma^{\sigma\sigma'}(k_1, k_2, k_3) \prod_{j=1}^4 G(k_j), \quad (77)$$

where $G(k)$ is the exact one-particle Green's function and $k_4 = k_1 + k_2 - k_3$.

At this point it is worthwhile to investigate the symmetries of the vertex function. A simple $SU(2)$ transformation shows that for a spin-rotation invariant system,

$$\Gamma^{\uparrow\uparrow} = (1 - X)\Gamma^{\uparrow\downarrow}, \quad (78)$$

where $X\Gamma(k_1, k_2, k_3) = \Gamma(k_2, k_1, k_3)$. Because the whole information is contained in the function $\Gamma^{\uparrow\downarrow}$, we will only consider the vertex of anti-parallel spins from now on and omit the spin indices (i.e. $\Gamma = \Gamma^{\uparrow\downarrow}$).

The permutation symmetry gives

$$\Gamma(k_1, k_2, k_3) = \Gamma(k_2, k_1, k_1 + k_2 - k_3). \quad (79)$$

Time reversal invariance, spin rotation invariance and parity imply

$$\Gamma(k_1, k_2, k_3) = \Gamma(k_1 + k_2 - k_3, k_3, k_2). \quad (80)$$

From the behavior under complex conjugation one obtains

$$\overline{\Gamma(k_1, k_2, k_3)} = \Gamma(\overline{k_1 + k_2 - k_3}, \overline{k_3}, \overline{k_2}), \quad (81)$$

where $\overline{k} = (-k_0, \mathbf{k})$. It follows that Γ is real if the frequencies are put to zero.

B Parquet diagrams: An example

A typical parquet diagram, is shown in Fig. 14. It is a p-p diagram embedded into a p-h 2. For simplicity, we choose the total momentum and the external frequencies k_0, k'_0 and Q_0 to be zero and we assume a constant coupling function g . In addition, we assume that \mathbf{Q} is a perfect nesting vector, such that $\xi_{\mathbf{q}+\mathbf{Q}} = -\xi_{\mathbf{q}}$. The value of the diagram (at $T \rightarrow 0$) is then

$$\frac{2g^3}{(\beta V)^2} \sum_{pq} C_\Lambda(q) C_\Lambda(q+Q) C_\Lambda(p) C_\Lambda(q-p+k). \quad (82)$$

After integration with respect to p_0 and q_0 , we obtain

$$(74) = -\frac{g^3}{V^2} \sum'_{\mathbf{p}, \mathbf{q}} \frac{\Theta(\xi_{\mathbf{p}} \xi_{\mathbf{q}-\mathbf{p}+\mathbf{k}})}{|\xi_{\mathbf{q}}|(|\xi_{\mathbf{q}}| + |\xi_{\mathbf{p}}| + |\xi_{\mathbf{q}-\mathbf{p}+\mathbf{k}}|)} = -\int_{\Lambda}^W d\xi \int_{2\Lambda}^W d\xi' \frac{\tilde{\nu}(\xi, \xi')}{|\xi|(|\xi| + |\xi'|)}, \quad (83)$$

where the sum $\sum'_{\mathbf{p}, \mathbf{q}}$ is over all momenta \mathbf{p} and \mathbf{q} allowed by the infrared cutoff and

$$\tilde{\nu}(\xi, \xi') = \frac{1}{V^2} \sum_{\mathbf{p}, \mathbf{q}} \delta(\xi - \xi_{\mathbf{q}}) \delta(\xi' - \xi_{\mathbf{p}} - \xi_{\mathbf{q}-\mathbf{p}+\mathbf{k}}) \Theta(\xi_{\mathbf{p}} \xi_{\mathbf{q}-\mathbf{p}+\mathbf{k}}). \quad (84)$$

If the Fermi level is not at a Van Hove singularity, $\tilde{\nu}(\xi, \xi')$ is usually bounded. Depending on the situation, $\tilde{\nu}$ could even be suppressed to zero for $\xi, \xi' \rightarrow 0$. This would reduce the singularity of the diagram in such a way that it can be neglected within the leading order approximation. The cases where parquet diagrams are most singular are those where $\tilde{\nu}(\xi, \xi')$ is positive for $\xi, \xi' \rightarrow 0$ (and can thus be approximated by a constant). It means that to leading order, our diagram is proportional to the following integral:

$$P(\Lambda) = \int_{\Lambda}^W \frac{d\xi}{\xi} \underbrace{\int_{\Lambda}^W \frac{d\xi'}{\xi + \xi'}}_{F_{\Lambda}(\xi)} = \frac{1}{2} \log^2 \frac{W}{\Lambda}. \quad (85)$$

For further convenience we have introduced the symbol $F_{\Lambda}(\xi)$ for the value of the internal p-p bubble. The result shows that indeed our diagram is of the leading order $g^3 \log^2 \Lambda$.

To obtain its contribution to the RG equation, we take the derivative with respect to Λ

$$-\partial_{\Lambda} P(\Lambda) = \frac{1}{\Lambda} F_{\Lambda}(\Lambda) + \int_{\Lambda}^W \frac{d\xi}{\xi(\xi + \Lambda)} \quad (86)$$

The first term is obtained by putting the large loop variable ξ to the energy scale Λ . The second term comes from the derivative of the internal p-p loop. A simple calculation leads us to two important observations:

1. The second term (equal to $\Lambda^{-1} \log \frac{2W}{W+\Lambda} \sim \Lambda^{-1}$) is negligible as compared to the first one ($\sim \Lambda^{-1} \log \Lambda$). This result can be generalized as follows. If a diagram is reducible in one channel, the dominant contributions to its Λ -derivative will be obtained by deriving only the propagators connecting the irreducible blocks and *not* the irreducible blocks themselves. This is exactly what we used in the derivation of the one-loop flow equations in section 7.
2. We can replace $F_{\Lambda}(\Lambda)$ in Eq. (86) by $F_{\Lambda}(0)$ without changing the result to leading order. In fact, integrating the simplified RG equation $-\partial_{\Lambda} P(\Lambda) = \frac{1}{\Lambda} F_{\Lambda}(0)$, we obtain indeed the correct result for $P(\Lambda)$. This result can be generalized as follows. In the RG equation, one can replace any vertex $\Gamma(k_1, k_2, k_3)$ by its value at $\xi_1 = \xi_2 = \xi_3 = 0$, i.e. the momenta k_i can be projected onto the Fermi surface. In this sense the dependence of the vertex on the band energies ξ_i is irrelevant. The same is true for its dependence on the frequencies. The replacement $F_{\Lambda}(\Lambda) \rightarrow F_{\Lambda}(0)$ is only justified in the differential RG equation Eq. (86), but *not* in the integral expression Eq. (85), since $\int_{\Lambda}^W d\xi / \xi F_{\Lambda}(0) = \log^2(W/\Lambda) \neq P(\Lambda)$. It is important to note that although the dependence of the vertex on the band energies and frequencies is irrelevant in the sense explained above, this dependence does not need to be weak at all! In our example, $F_{\Lambda}(\xi)$ depends clearly on ξ .

C Linear response

In this appendix, we investigate the linear response of the system to a weak external perturbation.

C.1 Generalized susceptibilities for superconductivity

Let the system be coupled to a time dependent, real valued field $\lambda(\mathbf{r}, t)$, via an additional term in the Hamiltonian

$$H_{\text{ext}, t} = - \sum_{\mathbf{r}} \lambda(\mathbf{r}, t) \left(\Delta_A(\mathbf{r}) + \Delta_A^\dagger(\mathbf{r}) \right), \quad (87)$$

where

$$\Delta_A(\mathbf{r}) = \sum_{\mathbf{r}'} f_A(\mathbf{r} - \mathbf{r}') c_{\mathbf{r}'\downarrow} c_{\mathbf{r}\uparrow}, \quad (88)$$

is the locally defined superconducting order parameter. The index A stands for the internal wave function $f_A(\mathbf{r} - \mathbf{r}')$ of the Cooper pair. This term can also be written in Fourier space as

$$H_{\text{ext}, t} = -V \sum_{\mathbf{k}} (\lambda(-\mathbf{k}, t) \Delta_A(\mathbf{k}) + \text{h. c.}), \quad (89)$$

where

$$\Delta_A(\mathbf{k}) = \sum_{\mathbf{r}} e^{-i\mathbf{kr}} \Delta_A(\mathbf{r}) = \sum_{\mathbf{p}} f_A(\mathbf{p}) c_{\mathbf{p}\downarrow} c_{\mathbf{k}-\mathbf{p}\uparrow} \quad (90)$$

and the functions $\lambda(\mathbf{k})$ and $f_A(\mathbf{p})$ are the Fourier transforms¹⁰ of $\lambda(\mathbf{r})$ and $f_A(\mathbf{r})$.

The coupling to the field induces in general a non-zero value of $\langle \Delta_B(\mathbf{r}) \rangle_t$, where the internal wave function f_B can be different from f_A . The linear response is given by the retarded response function or susceptibility $\chi_{\text{ret}, BA}^{BCS}(\mathbf{r} - \mathbf{r}', t - t')$, via

$$\langle \Delta_B(\mathbf{r}) \rangle_t = \int dt' \sum_{\mathbf{r}'} \chi_{\text{ret}, BA}^{BCS}(\mathbf{r} - \mathbf{r}', t - t') \lambda(\mathbf{r}', t') \quad (91)$$

or, after Fourier transformation in space and time,

$$\langle \Delta_B(\mathbf{k}) \rangle_\omega = \chi_{\text{ret}, BA}^{BCS}(\mathbf{k}, \omega) \lambda(\mathbf{k}, \omega). \quad (92)$$

The global superconducting order parameter is given by $\Delta(\mathbf{k} = 0)$.

A more convenient quantity is the Matsubara response function given by

$$\chi_{BA}^{BCS}(\mathbf{k}, \nu) = \frac{1}{V} \int_0^\beta d\tau e^{i\nu\tau} \left\langle \Delta_B(\mathbf{k}, \tau) \Delta_A^\dagger(\mathbf{k}) \right\rangle, \quad (93)$$

where the Bose-Matsubara frequency ν is restricted to even multiples of $2\pi/\beta$ and the imaginary time dependence of operators is given by Eq. (75). The retarded response function is obtained by analytic continuation

$$\chi(\nu) \xrightarrow{i\nu \rightarrow \omega + i\delta} \chi_{\text{ret}}(\omega), \quad (94)$$

where δ is an infinitesimal (dissipative) term.

¹⁰ We use the conventions $F(\mathbf{r}) = \frac{1}{V} \sum_{\mathbf{k}} e^{i\mathbf{kr}} F(\mathbf{k})$ and $F(\mathbf{k}) = \sum_{\mathbf{r}} e^{-i\mathbf{kr}} F(\mathbf{r})$ for any quantity $F(\mathbf{r})$. The only exceptions are the creation, and annihilation operators. There, we use a pre-factor $V^{-1/2}$ for both transformations. Note that $F^\dagger(\mathbf{k})$ denotes the Hermitian conjugate of $F(\mathbf{k})$ rather than the usual Fourier transform of $F^\dagger(\mathbf{r})$. The Fourier transform in (real) time is defined as $F(t) = \int \frac{d\omega}{2\pi} e^{-i\omega t} F(\omega)$ and $F(\omega) = \int dt e^{i\omega t} F(t)$.

Eq. (93) together with Eq. (77), give

$$\chi_{BA}^{BCS}(k) = \frac{1}{V} \int_0^\beta d\tau e^{i\nu\tau} \sum_{\mathbf{p}, \mathbf{p}'} f_B(\mathbf{p}) \overline{f_A(\mathbf{p}')} \left\langle c_{\mathbf{p}\downarrow}(\tau) c_{\mathbf{k}-\mathbf{p}\uparrow}(\tau) c_{\mathbf{k}-\mathbf{p}'\uparrow}^\dagger c_{\mathbf{p}'\downarrow}^\dagger \right\rangle \quad (95)$$

$$= \frac{1}{(\beta V)^2} \sum_{p, p'} f_B(\mathbf{p}) \overline{f_A(\mathbf{p}')} G^{\downarrow\uparrow}(p, k-p, k-p'), \quad (96)$$

$$= \frac{1}{(\beta V)^2} \sum_{p, p'} f_B(\mathbf{p}) [\beta V \delta_{p, p'} + D_k^{pp}(p) \Gamma_k^{BCS}(p, p')] D_k^{pp}(p') \overline{f_A(\mathbf{p}')}, \quad (97)$$

where $k = (\nu, \mathbf{k})$, $\Gamma_k^{BCS}(p, p') = \Gamma(p, k-p, k-p')$ and $\overline{f_A(\mathbf{p}')}$ is the complex conjugate of $f_A(\mathbf{p}')$.

It is argued at the end of section 3 that the low energy behavior in the weak coupling limit is determined by the degrees of freedom close to the Fermi surface. Therefore the dependence of the form factors on ξ is irrelevant. Let us perform the change of variables $\mathbf{p} \rightarrow \xi_{\mathbf{p}}, \theta_{\mathbf{p}}$, where ξ is the band energy and θ is a suitable (angular) variable. The most elementary superconducting susceptibility is a function of two angular variables, which is obtained by putting $f_B(\mathbf{p}) = \delta(\theta_{\mathbf{p}} - \theta)$ and $f_A(\mathbf{p}') = \delta(\theta_{\mathbf{p}'} - \theta')$ in Eq. (97),

$$\chi^{BCS}(k, \theta, \theta') = \int d\xi \int d\xi' J(\xi, \theta) J(\xi', \theta') \frac{1}{\beta^2} \sum_{p_0, p'_0} G^{\downarrow\uparrow}(p_{(\theta, \xi)}, k-p_{(\theta, \xi)}, k-p_{(\theta', \xi')}) \quad (98)$$

where $J(\xi, \theta)$ is the Jacobian, such that $1/V \sum_{\mathbf{p}} \rightarrow \int d\theta \int d\xi J(\xi, \theta)$.

This susceptibility allows to analyze the superconducting instability without any prejudice on the form factor $f(\mathbf{p})$. The natural form factor is obtained by writing $\chi(\theta, \theta')$ in diagonalized form

$$\chi(\theta, \theta') = \sum_n \chi_n f_n(\theta) f_n(\theta'), \quad (99)$$

where χ_n and f_n are, respectively, eigenvalues and eigenfunctions of the operator

$$f(\theta) \rightarrow \int d\theta' \chi(\theta, \theta') f(\theta'). \quad (100)$$

If χ_n diverges at an energy scale Λ_c , this indicates a (spin-, charge- or superconducting) instability with the form factor f_n .

To simplify the calculations, one often selects a certain form factor $f(\mathbf{p})$ and calculates the susceptibility for $f_A(\mathbf{p}) = f_B(\mathbf{p}) = f(\mathbf{p})$.

C.2 Density waves and flux phases

The effect of a term creating electron-hole pairs is evaluated in the same way as that of a two-particle source term. We consider operators of the form

$$\Delta(\mathbf{r}) = \frac{1}{2} \sum_{\mathbf{r}', \sigma} s_\sigma f(\mathbf{r}' - \mathbf{r}) c_{\mathbf{r}'\sigma}^\dagger c_{\mathbf{r}\sigma}, \quad (101)$$

or in Fourier space

$$\Delta(\mathbf{q}) = \frac{1}{2} \sum_{\mathbf{p}, \sigma} s_\sigma f(\mathbf{p}) c_{\mathbf{p}\sigma}^\dagger c_{\mathbf{p}+\mathbf{q}\sigma}. \quad (102)$$

The most simple cases are the magnetization ($s_\sigma = \sigma$) and the charge ($s_\sigma = 1$), where $f(\mathbf{p}) = 1$, but many possibilities with non-trivial \mathbf{p} -dependencies exist. Two other examples: if $f(\mathbf{p})$ is a function with

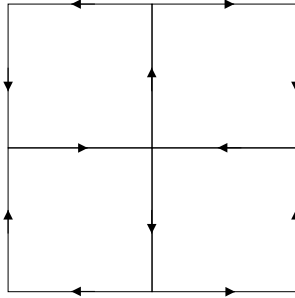


Fig. 15 The pattern of charge (spin) currents along the bonds of the square lattice in a charge (spin) flux-phase

$d_{x^2-y^2}$ -symmetry, $\mathbf{q} = (\pi, \pi)$ and $s_\sigma = 1$ (σ), then the nearest-neighbor-terms in $\langle \Delta(\mathbf{q}) \rangle$ yield circular charge (spin) currents flowing around the plaquettes of the square lattice with alternating directions (see Fig. 15). These charge and spin instabilities have been discussed a long time ago in the context of the excitonic insulator [HR68].

The phase with circulating charge currents is actually identical to the flux-phase [AM88, Kot88] and sometimes referred to as d -density wave, charge-current wave or orbital antiferromagnetism. Recently this order parameter was proposed to compete with d -wave superconductivity and to be responsible for the pseudo gap phase of the cuprates [CLMN01].

The phase with circulating spin currents is called the spin flux-phase. Other names encountered in the literature are “spin current wave” or “spin nematic state” (because it is a state with broken rotational symmetry and unbroken time reversal symmetry). The low-temperature thermodynamics of both charge and spin flux-phases have been investigated in mean field approximation in Refs. [NV89, NJK91].

We again considered two different form factors f_A and f_B . This allows either to obtain an “angle-resolved” susceptibility $\chi^{s/c}(q, \theta, \theta')$ in analogy to Eq. (98), or to select the form factor f in advance and to choose $f_A = f_B = f$. The generalized charge- and spin susceptibilities are given by

$$\chi_{BA}^{s/c}(q) = \frac{1}{V} \int_0^\beta d\tau e^{i\nu\tau} \left\langle \Delta_B(\mathbf{q}, \tau) \left(\Delta_A^\dagger(\mathbf{q}) + \Delta_A(-\mathbf{q}) \right) \right\rangle \quad (103)$$

$$= \frac{1}{4V} \int_0^\beta d\tau e^{i\nu\tau} \sum_{\mathbf{p}, \mathbf{p}'} f_B(\mathbf{p}) \left(\overline{f_A(\mathbf{p}')} + f_A(\mathbf{p}' + \mathbf{q}) \right) \cdot \\ \cdot \sum_{\sigma\sigma'} s_\sigma s_{\sigma'} \left\langle c_{\mathbf{p}\sigma}^\dagger(\tau) c_{\mathbf{p}+\mathbf{q}\sigma}(\tau) c_{\mathbf{p}'+\mathbf{q}\sigma'}^\dagger c_{\mathbf{p}'\sigma'} \right\rangle, \quad (104)$$

where $q = (\nu, \mathbf{q})$. The most prominent case is $\mathbf{q} = (\pi, \pi)$, where $\Delta_{A/B}(\mathbf{q})$ can be made Hermitian if we choose $f(\mathbf{p} + \mathbf{q}) = \overline{f(\mathbf{p})}$. With this choice the spin- and charge susceptibilities can be written in perfect analogy with Eq. (97)

$$\chi_{BA}^{s/c}(q) = \frac{1}{(\beta V)^2} \sum_{p, p'} f_B(\mathbf{p}) \overline{f_A(\mathbf{p}')} (G^{\uparrow\uparrow}(p', p + q, p) \mp G^{\uparrow\downarrow}(p', p + q, p)). \quad (105)$$

$$= \frac{1}{(\beta V)^2} \sum_{p, p'} f_B(\mathbf{p}) \left[-\beta V \delta_{p, p'} + D_q^{ph}(p) \Gamma_q^{s/c}(p, p') \right] D_q^{ph}(p') \overline{f_A(\mathbf{p}')}, \quad (106)$$

where $\Gamma_q^s(p, p') = -X\Gamma(p', p + q, p)$ and $\Gamma_q^c(p, p') = (2 - X)\Gamma(p', p + q, p)$.

C.3 Flow equations for the susceptibilities

The RG formalism can be used to calculate the susceptibilities to leading order in the infrared cutoff Λ . To see this, we rewrite Eqs. (97) and (106) as

$$\chi_{BA,\Lambda}^{BCS}(k) = \frac{1}{\beta V} \sum_p Z_{B,\Lambda,k}^{BCS}(p) D_{\Lambda,k}^{pp}(p) f_A(\mathbf{p}) \quad (107)$$

$$\chi_{BA,\Lambda}^{s/c}(q) = -\frac{1}{\beta V} \sum_p Z_{B,\Lambda,q}^{s/c}(p) D_{\Lambda,q}^{ph}(p) f_A(\mathbf{p}), \quad (108)$$

where the effective field vertices Z are defined as

$$Z_{B,\Lambda,k}^{BCS}(p) = f_B(\mathbf{p}) + \frac{1}{\beta V} \sum_{p'} f_B(\mathbf{p}') D_{\Lambda,k}^{pp}(p') \Gamma_{\Lambda,k}^{BCS}(p', p) \quad (109)$$

$$Z_{B,\Lambda,q}^{s/c}(p) = f_B(\mathbf{p}) - \frac{1}{\beta V} \sum_{p'} f_B(\mathbf{p}') D_{\Lambda,q}^{ph}(p') \Gamma_{\Lambda,q}^{s/c}(p', p). \quad (110)$$

The vertex function Γ^{BCS} in Eq. (109) can be expressed by an infinite series in the p-p irreducible part I^{pp} . Formally

$$\begin{aligned} Z_B^{BCS} &= f_B + f_B D^{pp} \Gamma^{BCS} \\ &= f_B + f_B D^{pp} I^{pp} + f_B D^{pp} I^{pp} D^{pp} I^{pp} + \dots \\ &= f_B + Z_B^{BCS} D^{pp} I^{pp} \end{aligned} \quad (111)$$

To get the flow equation, we take the derivative with respect to Λ of Eq. (111). It gives three terms

$$\dot{Z}_B^{BCS} = \dot{Z}_B^{BCS} D^{pp} I^{pp} + Z_B^{BCS} \dot{D}^{pp} I^{pp} + Z_B^{BCS} D^{pp} \dot{I}^{pp}. \quad (112)$$

The last term of Eq. (112) is neglected for the same reason as in Eqs. (42). The remaining equation is iterated to give

$$\begin{aligned} \dot{Z}_B^{BCS} &= Z_B^{BCS} \dot{D}^{pp} I^{pp} + Z_B^{BCS} \dot{D}^{pp} I^{pp} D^{pp} I^{pp} + Z_B^{BCS} \dot{D}^{pp} I^{pp} D^{pp} I^{pp} D^{pp} I^{pp} + \dots \\ &= Z_B^{BCS} \dot{D}^{pp} \Gamma^{BCS} \end{aligned} \quad (113)$$

This is the RG equation for the field-vertex Z_B^{BCS} . The form factor f_B enters as an initial condition $Z_{B,\Lambda_0,k}^{BCS}(p) \approx f_B(\mathbf{p})$.

It is now easy to obtain a RG equation for χ^{BCS} as well. From Eqs. (107) and (113)

$$\begin{aligned} \dot{\chi}^{BCS} &= \dot{Z}_B^{BCS} D^{pp} f_A + Z_B^{BCS} \dot{D}^{pp} f_A \\ &= Z_B^{BCS} \dot{D}^{pp} \Gamma^{BCS} D^{pp} f_A + Z_B^{BCS} \dot{D}^{pp} f_A \\ &= Z_B^{BCS} \dot{D}^{pp} (f_A + \Gamma^{BCS} D^{pp} f_A) \\ &= Z_B^{BCS} \dot{D}^{pp} Z_A^{BCS} \end{aligned} \quad (114)$$

In the last equation, we have introduced the function $Z_{A,\Lambda,k}^{BCS}(p)$, which is the same as $Z_{B,\Lambda,k}^{BCS}(p)$, except that the initial condition $f_B(\mathbf{p})$ is changed into $f_A(\mathbf{p})$.

Written out, the RG equations for the pairing susceptibility are

$$\dot{\chi}_{BA,\Lambda}^{BCS}(k) = \frac{1}{\beta V} \sum_p Z_{B,\Lambda,k}^{BCS}(p) \dot{D}_{\Lambda,k}^{pp}(p) Z_{A,\Lambda,k}^{BCS}(p) \quad (115)$$

$$\dot{Z}_{\diamond,\Lambda,k}^{BCS}(p) = \frac{1}{\beta V} \sum_{p'} Z_{\diamond,\Lambda,k}^{BCS}(p') \dot{D}_{\Lambda,k}^{pp}(p') \Gamma_{\Lambda,k}^{BCS}(p', p), \quad (116)$$

where $\diamond = A$ or B , and $\Gamma_{\Lambda,k}^{BCS}(p', p) = \Gamma_{\Lambda}(p', k - p', k - p)$.

Once the vertex function Γ^{BCS} is known from the one-loop RG equation, one can solve the linear equation (116) for the initial condition $Z_{\diamond, \Lambda_0, k}^{BCS}(p) = f_{\diamond}(\mathbf{p})$ and finally one can integrate Eq. (115) to obtain the susceptibility.

All the steps can be repeated for the charge- and spin susceptibilities, just by replacing the quantities $Z^{BCS}, \Gamma^{BCS}, I^{pp}$ by $Z^{s/c}, \Gamma^{s/c}, I^{s/c}$ and the p-p propagator D^{pp} by $-D^{ph}$.

$$\dot{\chi}_{BA, \Lambda}^{s/c}(q) = -\frac{1}{\beta V} \sum_p Z_{B, \Lambda, q}^{s/c}(p) \dot{D}_{\Lambda, q}^{ph}(p) Z_{A, \Lambda, q}^{s/c}(p) \quad (117)$$

$$\dot{Z}_{\diamond, \Lambda, q}^{s/c}(p) = -\frac{1}{\beta V} \sum_{p'} Z_{\diamond, \Lambda, q}^{s/c}(p') \dot{D}_{\Lambda, q}^{ph}(p') \Gamma_{\Lambda, q}^{s/c}(p', p), \quad (118)$$

where $\diamond = A$ or B , $\Gamma_{\Lambda, q}^s(p', p) = -X\Gamma_{\Lambda}(p', p + q, p)$ and $\Gamma_{\Lambda, q}^c(p', p) = (2 - X)\Gamma_{\Lambda}(p', p + q, p)$.

D Functional integral formulation

In the functional integral formulation the annihilation- and creation operators $c_{\mathbf{k}\sigma}$ and $c_{\mathbf{k}\sigma}^{\dagger}$ are replaced by anti-commuting Grassmann fields $\psi_{(\tau, \mathbf{k}, \sigma)}$ and $\bar{\psi}_{(\tau, \mathbf{k}, \sigma)}$. They depend on the “imaginary time” variable $\tau \in [0, \beta]$ in addition to the labels of the single-particle states and they satisfy anti-periodic boundary conditions in the τ variable.

The Hamilton operator is transformed into the action

$$S[\psi] = - \int_0^\beta d\tau \left(\sum_{\mathbf{k}\sigma} \bar{\psi}_{(\tau, \mathbf{k}, \sigma)} (\partial_\tau - \mu) \psi_{(\tau, \mathbf{k}, \sigma)} + H[\tau, \psi] \right), \quad (119)$$

where $H[\tau, \psi]$ is obtained from the Hamiltonian by the replacements $c_{\mathbf{k}\sigma} \rightarrow \psi_{(\tau, \mathbf{k}, \sigma)}$ and $c_{\mathbf{k}\sigma}^{\dagger} \rightarrow \bar{\psi}_{(\tau, \mathbf{k}, \sigma)}$.

It is useful to take the Fourier transform

$$\psi_{\sigma k} = \beta^{-1/2} \int_0^\beta d\tau e^{ik_0\tau} \psi_{(\tau, \mathbf{k}, \sigma)}, \quad (120)$$

where $k = (k_0, \mathbf{k})$ contains the Matsubara frequency k_0 . It allows to write the action as

$$S[\psi] = S_0[\psi] - W[\psi], \quad (121)$$

with

$$S_0[\psi] = \sum_{\sigma, k} \bar{\psi}_{\sigma k} (ik_0 - \xi_{\mathbf{k}}) \psi_{\sigma k}, \quad (122)$$

where $\xi_{\mathbf{k}} = e_{\mathbf{k}} - \mu$ and

$$W[\psi] = \frac{1}{2} \frac{1}{\beta V} \sum_{k_1, k_2, k_3} g(\mathbf{k}_1, \mathbf{k}_2, \mathbf{k}_3) \sum_{\sigma, \sigma'} \bar{\psi}_{k_1 \sigma} \bar{\psi}_{k_2 \sigma'} \psi_{k_3 \sigma'} \psi_{k_1 + k_2 - k_3 \sigma}. \quad (123)$$

The partition function is given by the functional integral

$$Z = \int \mathcal{D}\psi e^{S[\psi]}, \quad (124)$$

where $\mathcal{D}\psi$ is a short-hand notation for $\prod_{k\sigma} d\psi_{k\sigma} d\bar{\psi}_{k\sigma}$.

The one- and two-particle Green's functions are given by

$$G(k) = -\langle \psi_{k\sigma} \bar{\psi}_{k\sigma} \rangle \quad (125)$$

$$G^{\sigma\sigma'}(k_1, k_2, k_3) = \beta V \langle \psi_{k_1\sigma} \psi_{k_2\sigma'} \bar{\psi}_{k_3\sigma'} \bar{\psi}_{k_1+k_2-k_3\sigma} \rangle. \quad (126)$$

where the average of a Grassmann expression $O[\psi]$ is defined as

$$\langle O[\psi] \rangle = \frac{1}{Z} \int \mathcal{D}\psi e^{S[\psi]} O[\psi]. \quad (127)$$

It is convenient to introduce the partition function with source term

$$Z[\eta] = \int d\mu_C[\psi] e^{-W[\psi] + (\bar{\eta}, \psi) + (\bar{\psi}, \eta)}, \quad (128)$$

where we used the short-hand notation $(\bar{\chi}, \psi) := \sum_{\sigma k} \bar{\chi}_{\sigma k} \psi_{\sigma k}$ and the normalized Gaussian measure is defined by

$$d\mu_C[\psi] := \frac{\mathcal{D}\psi e^{(\bar{\psi}, C^{-1}\psi)}}{\int \mathcal{D}\psi e^{(\bar{\psi}, C^{-1}\psi)}}. \quad (129)$$

The connected part of the average of any Grassmann monomial is obtained as a functional derivative [NO88]

$$\langle \psi_1 \cdots \psi_n \bar{\psi}_{n+1} \cdots \bar{\psi}_{2n} \rangle_c = \frac{\delta^{2n} \log Z[\eta]}{\delta \eta_{2n} \cdots \delta \eta_{n+1} \delta \bar{\eta}_n \cdots \delta \bar{\eta}_1} \Big|_{\eta=0}, \quad (130)$$

where we have written ψ_i instead of $\psi_{k_i\sigma_i}$.

References

- [Abr65] A. A. Abrikosov. *Physics*, 2:5, 1965.
- [AGD61] A. A. Abrikosov, L. P. Gor'kov, and I. E. Dzyaloshinskii. *Methods of quantum field theory in statistical physics*. Prentice-Hall, 1961.
- [AM88] I. Affleck and J. B. Marston. *Phys. Rev. B*, 37:3774, 1988.
- [Aue94] A. Auerbach. *Interacting electrons and quantum magnetism*. Springer Verlag, 1994.
- [BB02] B. Binz, D. Baeriswyl, and B. Douçot. *Eur. Phys. J. B*, 25:69, 2002.
- [BG91] G. Benfatto and G. Gallavotti. *J. Stat. Phys.*, 59:541, 1991.
- [BGD66] Y. A. Bychkov, L. P. Gor'kov, and I. E. Dzyaloshinskii. *Sov. Phys. JEPT*, 23:489, 1966.
- [Bin02] B. Binz. PhD thesis, Université de Fribourg (Switzerland) and Université Paris VII, 2002.
- [BS89] N. E. Bickers and D. J. Scalapino. *Ann. Phys.*, 193:206, 1989.
- [BSW89] N. E. Bickers, D. J. Scalapino, and S. R. White. *Phys. Rev. Lett.*, 62:961, 1989.
- [CFS96] T. Chen, J. Fröhlich, and M. Seifert. In *Proceedings of the Les Houches Summer School*, page 913. Elsevier Science B. V., 1996.
- [CLMN01] S. Chakravarty, R. B. Laughlin, D. K. Morr, and C. Nayak. *Phys. Rev. B*, 63:94503, 2001.
- [CS95] G. Y. Chitov and D. Sénéchal. *Phys. Rev. B*, 52:129, 1995.
- [CS98] G. Y. Chitov and D. Sénéchal. *Phys. Rev. B*, 57:1444, 1998.
- [DD03] S. Dusuel and B. Douçot. *Phys. Rev. B*, 67:205111, 2003.
- [DK72] I. Dzyaloshinskii and E. I. Kats. *Zh. Eksp. Teor. Fiz.*, 62:1104, 1972. [Sov. Phys. JEPT **35**, 584 (1972)].
- [DR00] M. Disertori and V. Rivasseau. *Phys. Rev. Lett.*, 85:361, 2000.
- [Dup98] N. Dupuis. *Eur. Phys. J. B*, 3:315, 1998.
- [Dup00] N. Dupuis. *Int. J. Mod. Phys. B*, 14:379, 2000.

- [DVdA02] S. Dusuel and J. and B. Douçot Vistulo de Abreu. *Phys. Rev. B*, 65:94505, 2002.
- [Dzy96] I. Dzyaloshinskii. *J. Phys. I*, 6:119, 1996.
- [Eme79] V. J. Emery. *Highly conducting one-dimensional solids*. Plenum, 1979.
- [Faz99] P. Fazekas. *Lecture notes on electron correlation and magnetism*. World Scientific, Singapore, 1999.
- [Fer03] A. Ferraz. *Europhys. Lett.*, 61:228, 2003.
- [FST96] J. Feldman, M. Salmhofer, and E. Trubowitz. *J. Stat. Phys.*, 84:1209, 1996.
- [FST98] J. Feldman, M. Salmhofer, and E. Trubowitz. *Commun. Pure. Appl. Math.*, 51:1133, 1998.
- [FST99] J. Feldman, M. Salmhofer, and E. Trubowitz. *Commun. Pure. Appl. Math.*, 52:273, 1999.
- [FT90] J. Feldman and E. Trubowitz. *Helv. Phys. Acta*, 63:156, 1990.
- [FW71] A. L. Fetter and J. D. Walecka. *Quantum Theory of many particle systems*. McGraw-Hill, 1971.
- [GD74] L. P. Gor'kov and I. Dzyaloshinskii. *Zh. Eksp. Teor. Fiz.*, 67:397, 1974. [Sov. Phys. JEPT **40**, 198 (1975)].
- [GM54] M. and F. Low Gell-Mann. *Phys. Rev.*, 95:1300, 1954.
- [HM00] C. J. Halboth and W. Metzner. *Phys. Rev. B*, 61:7364, 2000.
- [HM01] C. J. Halboth and W. Metzner. *Phys. Rev. Lett.*, 85:5162, 2001.
- [Hon01] C. Honerkamp. *Eur. Phys. J. B*, 21:81, 2001.
- [HR68] B. I. Halperin and T. M. Rice. In F. Seitz, D. Turnbull, and H. Ehrenreich, editors, *Solid State Physics*, volume 21, page 116. Academic Press, New York, 1968.
- [HS01a] C. Honerkamp and M. Salmhofer. *Phys. Rev. B*, 64:184516, 2001.
- [HS01b] C. Honerkamp and M. Salmhofer. *Phys. Rev. Lett.*, 87:187004, 2001.
- [HS03] C. Honerkamp and M. Salmhofer. *Phys. Rev. B*, 67:174504, 2003.
- [HSFR01] C. Honerkamp, M. Salmhofer, N. Furukawa, and T. M. Rice. *Phys. Rev. B*, 63:35109, 2001.
- [HU02] C. Heidbrink and G. Uhrig. *Eur. Phys. J. B*, 30:443, 2002.
- [HW03] V. Hankevych and F. Wegner. *Eur. Phys. J. B*, 31:333, 2003.
- [IK01] V. Yu. Irkhin and A. A. Katanin. *Phys. Rev. B*, 64:205105, 2001.
- [IKK01] V. Yu. Irkhin, A. A. Katanin, and M. I. Katsnelson. *Phys. Rev. B*, 64:165107, 2001.
- [Keh01] S. Kehrein. *Nucl. Phys. B*, 592:512, 2001.
- [KL65] W. Kohn and J. M. Luttinger. *Phys. Rev. Lett.*, 15:524, 1965.
- [KM99] H. Kondo and T. Moriya. *J. Phys. Soc. Jap.*, 68:3170, 1999.
- [Kot88] G. Kotliar. *Phys. Rev. B*, 37:3664, 1988.
- [LK03] S. Ledowski and P. Kopietz. *J. Phys. C*, 15:4779, 2003.
- [Mor94] T. R. Morris. *Int. J. Mod. Phys. A*, 9:2411, 1994.
- [MP92] P. Monthoux and D. Pines. *Phys. Rev. Lett.*, 69:961, 1992.
- [MTU90] T. Moriya, Y. Takahashi, and K. Ueda. *J. Phys. Soc. Jap.*, 59:2905, 1990.
- [NGR69] P. Nozières, J. Gavoret, and B. Roulet. *Phys. Rev.*, 178:1084, 1969.
- [NJK91] A. A. Nersesyan, G. I. Japaridze, and I. G. Kimeridze. *J. Phys. C*, 3:3353, 1991.
- [NM03] A. Neumayr and W. Metzner. *Phys. Rev. B*, 67:35, 2003.
- [NO88] J. W. Negele and H. Orland. *Quantum Many-Particle Systems*. Addison-Wesley, 1988.
- [Noz64] P. Nozières. *Theory of interacting Fermi systems*. Addison Wesley, 1964.
- [NV89] A. A. Nersesyan and G. E. Vachnadze. *J. of Low Temp. Physics*, 77:293, 1989.
- [NW99] R. M. Noack and S. R. White. In I. Peschel et al., editors, *Density matrix renormalization: a new numerical method in physics*. Springer Verlag, Berlin, 1999.
- [Pol84] J. Polchinski. *Nucl. Phys. B*, 231:269, 1984.
- [Pol92] J. Polchinski. In *Proceedings of the 1992 TASI in Elementary Particle Physics*. World Scientific, 1992.
- [PSTM56] I. Y. Pomeranchuk, V. V. Sudakov, and K. A. Ter-Martirosian. *Phys. Rev.*, 103:784, 1956.
- [RGN69] B. Roulet, J. Gavoret, and P. Nozières. *Phys. Rev.*, 178:1072, 1969.
- [RPKW03] A. Rosch, J. Paaske, J. Kroha, and P. Wölfle. *Phys. Rev. Lett.*, 90:76, 2003.
- [Sal98] M. Salmhofer. *Commun. Math. Phys.*, 194:249, 1998.
- [SB51] E. E. Salpeter and H. A. Bethe. *Phys. Rev.*, 84:1232, 1951.
- [SH01] M. Salmhofer and C. Honerkamp. *Prog. Theor. Phys.*, 105:1, 2001.
- [Sha94] R. Shankar. *Rev. Mod. Phys.*, 66:129, 1994.
- [SP53] E. Stückelberg and A. Petermann. *Helv. Phys. Acta*, 26:499, 1953.
- [TW94] N. Tetradis and C. Wetterich. *Nucl. Phys. B*, 422:541, 1994.
- [VdA01] F. and B. Douçot Vistulo de Abreu. *Phys. Rev. Lett.*, 86:2866, 2001.
- [Weg94] F. Wegner. *Annalen der Physik (Leipzig)*, 3:77, 1994.
- [Wet93] C. Wetterich. *Phys. Lett. B*, 301:90, 1993.
- [Wil71] K. G. Wilson. *Phys. Rev. B*, 4:3174 and 3184, 1971.
- [Wil75] K. G. Wilson. *Rev. Mod. Phys.*, 47:773, 1975.
- [WK74] K. G. Wilson and J. Kogut. *Phys. Rep.*, 12C:75, 1974.
- [Zan96] D. Zanchi. PhD thesis, Université de Paris-Sud, Orsay, 1996.
- [Zan01] D. Zanchi. *Europhys. Lett.*, 55:376, 2001.
- [ZS96] D. Zanchi and H. J. Schulz. *Phys. Rev. B*, 54:9509, 1996.
- [ZS00] D. Zanchi and H. J. Schulz. *Phys. Rev. B*, 61:13609, 2000.
- [ZYD97] A. T. Zheleznyak, V. M. Yakovenko, and I. E. Dzyaloshinskii. *Phys. Rev. B*, 55:3200, 1997.